2018

Recent advances in Dirac spin-gapless semiconductors

Xiaotian Wang
University of Wollongong, xw573@uowmail.edu.au

Tingzhou Li
Southwest University

Zhenxiang Cheng
University of Wollongong, cheng@uow.edu.au

Xiaolin Wang
University of Wollongong, xiaolin@uow.edu.au

Hong Chen
Southwest University

Publication Details

Wang, X., Li, T., Cheng, Z., Wang, X. & Chen, H. (2018). Recent advances in Dirac spin-gapless semiconductors. Applied Physics Reviews, 5 (4), 041103-1-041103-19.

Recent advances in Dirac spin-gapless semiconductors

Abstract
Spin-gapless semiconductors (SGSs), the new generation of spintronic materials, have received increasing attention recently owing to their various attractive properties such as fully spin-polarization and high carrier mobility. Based on their unique band structures, SGSs can be divided into two types: parabolic and Dirac-like linear. The linear-type SGSs, also called Dirac SGSs (DSGSs), have real massless fermions and dissipation-less transport properties, and thus are regarded as promising material candidates for applications in ultra-fast and ultra-low-power spintronic devices. DSGSs can be further classified into p-state type or d-state type depending on the degree of contribution of either the p-orbitals or d-orbitals to the Dirac states. Considering the importance of the research field and to cover its fast development, we reviewed the advances in DSGSs and proposed our own viewpoints. First, we introduced the computational algorithms of SGSs. Second, we found that the boundaries between DSGSs and Dirac half-metals were frequently blurred. Therefore, a simple classification is proposed in this work. Third, we collected almost all the studies on DSGSs published in the past six years. Finally, we proposed new guidance to search for DSGSs among 3D bulk materials on the basis of our latest results.

Disciplines
Engineering | Physical Sciences and Mathematics

Publication Details
Wang, X., Li, T., Cheng, Z., Wang, X. & Chen, H. (2018). Recent advances in Dirac spin-gapless semiconductors. Applied Physics Reviews, 5 (4), 041103-1-041103-19.

Recent advances in Dirac spin-gapless semiconductors

Xiaotian Wang, Tingzhou Li, Zhenxiang Cheng, Xiao-Lin Wang, and Hong Chen

Citation: Applied Physics Reviews **5**, 041103 (2018); doi: 10.1063/1.5042604
View online: https://doi.org/10.1063/1.5042604
View Table of Contents: http://aip.scitation.org/toc/are/5/4
Published by the American Institute of Physics

APPLIED PHYSICS REVIEWS—FOCUSED REVIEW

Recent advances in Dirac spin-gapless semiconductors

Xiaotian Wang,[1,2,a)] Tingzhou Li,[1,a)] Zhenxiang Cheng,[2,b)] Xiao-Lin Wang,[2] and Hong Chen[1,b)]
[1]*School of Physical Science and Technology, Southwest University, Chongqing 400715, People's Republic of China*
[2]*Institute for Superconducting & Electronic Materials and ARC Centre of Excellence in Future Low-Energy Electronics Technologies, University of Wollongong, Wollongong 2500, Australia*

(Received 2 June 2018; accepted 1 August 2018; published online 17 October 2018)

Spin-gapless semiconductors (SGSs), the new generation of spintronic materials, have received increasing attention recently owing to their various attractive properties such as fully spin-polarization and high carrier mobility. Based on their unique band structures, SGSs can be divided into two types: parabolic and Dirac-like linear. The linear-type SGSs, also called Dirac SGSs (DSGSs), have real massless fermions and dissipation-less transport properties, and thus are regarded as promising material candidates for applications in ultra-fast and ultra-low-power spintronic devices. DSGSs can be further classified into *p*-state type or *d*-state type depending on the degree of contribution of either the *p*-orbitals or *d*-orbitals to the Dirac states. Considering the importance of the research field and to cover its fast development, we reviewed the advances in DSGSs and proposed our own viewpoints. First, we introduced the computational algorithms of SGSs. Second, we found that the boundaries between DSGSs and Dirac half-metals were frequently blurred. Therefore, a simple classification is proposed in this work. Third, we collected almost all the studies on DSGSs published in the past six years. Finally, we proposed new guidance to search for DSGSs among 3D bulk materials on the basis of our latest results. *Published by AIP Publishing.* https://doi.org/10.1063/1.5042604

TABLE OF CONTENTS

I. INTRODUCTION

Spintronics, a promising research field, focuses mainly on one degree of freedom of the electron, namely, spin. Traditional electronic devices have high power consumption and relatively low circuit integration, leading to physical limitations. Spintronics aims to manipulate the spin degree to obtain faster transport and dissipation-less properties. However, there are still many issues to be resolved, such as the generation and injection of the spin-polarized carrier, the manipulation and detection of the spin direction, and the long-distance spin-polarized transport.[1–3] Researchers have proposed various concepts or spintronic materials to address these problems, including half-metals (HMs),[4–8] topological insulators (TIs),[9–14] magnetic semiconductors (MSs),[15–18] and spin-gapless semiconductors (SGSs).

The first SGS was proposed by Wang[19] on the basis of first-principles calculations in 2008. During the past ten years, many 2D and 3D bulk SGSs[19–43] have been predicted theoretically; however, most of SGSs that have been synthesized were Heusler-based compounds, such as Mn_2CoAl,[20] CoFeCrGa,[32] and CoFeMnSi,[33] whereas there has been barely any experimental work on 2D materials. Owing to the special zero-band-gap character of SGSs, these types of

[a)]X. Wang and T. Li contributed equally to this work.
[b)]Authors to whom correspondence should be addressed: cheng@uow.edu.au and chenh@swu.edu.cn

materials have many novel properties, some of which are listed as follows:[19] (i) only a tiny amount of energy is required to excite electrons from the valence band to the conduction band; (ii) the excited charge carriers, both electrons and holes, can be 100% spin-polarized simultaneously; (iii) using the Hall effect, fully spin-polarized electrons and holes can be easily separated. Most of the SGSs predicted so far possess parabolic energy dispersions.

However, the ultimate goals for future spintronic or electronic devices are to achieve ultra-fast transport and ultra-low-energy-consumption.[2] That is, we ideally need to eliminate the (effective) mass of electrons or holes and to make the massless charges completely spin-polarized. Therefore, compared with parabolic-like SGSs (PSGSs), Dirac-like SGSs (DSGSs) are the better class of spintronic materials for use in spintronic devices owing to their Dirac dispersion. Specifically, DSGSs have a graphene-like linear energy dispersion; owing to this unique dispersion, the (effective) mass of the electrons can be eliminated. Normally, DSGSs can be divided into two types: type I, the *d*-state DSGSs, in which the Dirac state is contributed by *d*-orbitals of transition-metal (TM) atoms, and type II, the *p*-state DSGSs, where it is contributed by *p*-orbitals of main-group (MG) atoms. Overall, as a member of a topological non-trivial family, DSGSs have 100% spin-polarization, high Fermi velocity (v_F), massless fermions around the Fermi level, and dissipation-less properties. All of these desirable properties indicate that they may have applications in high-efficiency spintronic devices in the future. Graphene, which has a similar Dirac band structure to that of the DSGSs, has been fully investigated in the past decade; however, its Dirac cone is intrinsically spin-degenerated, which actually limited its utilization in some fields of spintronics. Beyond graphene, some studies have found that the Dirac state does exist in some similar original two-dimensional materials such as silicene,[44] phosphorene,[45] TiB_2 monolayers,[46] and germanene.[47] With the old generation of Dirac-type materials, there was no suitable method to balance the existence of Dirac states and other necessary properties such as magnetism through doping. By contrast, the DSGSs do not require any external conditions to overcome these practical obstacles. Thus, it is highly desirable to find stable new DSGSs with an intrinsic 100% spin-polarized Dirac state.

In this article, we will not only review recent research on the DSGSs but also present our own viewpoints. While collecting publications on DSGSs, we noted that the concept of DSGS was very often confused with that of Dirac HMs (DHMs), owing to their similar band structures around the Fermi level. Therefore, in this paper, we propose a better understanding of both concepts for easy delineation of the two types of materials. On the other hand, a major limitation is that none of the predicted 2D DSGSs has yet been successfully prepared experimentally. Therefore, it is necessary to find a new approach for searching stable and easily synthesizable DSGS materials. Based on our recent study, we found that there exists a novel quasi-linear dispersion in bulk Heusler compounds. Thus, we speculate that the Dirac states may also exist in such stable bulk Heusler compounds.

II. COMPUTATIONAL METHODS

In SGSs or other novel spintronic materials under investigation, the Density Functional Theory[48] (DFT) has become the most popular and versatile method. Owing to the help of DFT and first-principles, the physical properties of novel materials can be designed and described with solely the input of physical constants. Normally, the first and one of the most important steps in first-principles studies is properly preparing the objective structures. Usually, a supercell of materials is needed to be created for the simulation, after constructing the supercell, geometry optimization is performed on the structures on the basis of DFT. To date, several DFT packages, i.e., Dmol^3,[49] Spanish Initiative for Electronic Simulations with Thousands of Atoms (SIESTA),[50] Vienna *Ab-initio* Simulation Package (VASP),[51] and Cambridge Sequential Total Energy Package (CASTEP)[52] and so on, can give information towards total energies, forces, and stresses on an atomic system, as well as perform geometry optimization, electronic structure calculations, optical spectra drawing, and molecular dynamics simulations. Among them, Dmol^3 and SIESTA are composed of atomic orbital basis sets, however, the VASP, CASTEP, ABINIT,[53] and Quantum Espresso (QE)[54] are based on plane-wave basis sets for periodic systems.

In this section, the merits of above-mentioned packages are described briefly: for the VASP, it uses the projector-augmented wave method or ultra-soft pseudo-potentials and therefore, the size of the basis-set can be kept very small even for TMs and first-row elements such as C and O. For the QE, it is based on the plane-wave self-consistent field program where both DFT and density functional perturbation theory are included, using plane-wave basis sets and pseudo-potentials. For the Dmol^3, it has long been one of the fastest methods for molecular DFT calculations due to its unique approach to electrostatics. It can quickly perform structure optimization of molecular systems using delocalized internal coordinates. For the CASTEP, it employs the DFT plane-wave pseudo-potentials method, which can simulate a wide range of the properties of crystals and surfaces in materials such as semiconductors, ceramics, metals, minerals, and zeolites.

Several levels of approximations, including the local density approximation (LDA)[55] and the generalized gradient approximation (GGA),[56] are widely accepted in calculations involving 2D and 3D materials. Two of the most widely used GGA functional in such calculations are the Perdew-Wang functional (PW91)[57] and the Perdew-Burke-Ernzerhof functional (PBE).[58] Tas *et al.*[59] revealed that DFT calculations using GGA-PBE gave a fair description of the electronic properties of PSGSs. However, the GGA method still has some failures: (i) GGA may be not adequate for more complicated systems; (ii) the GGA is plagued by large band-gap errors in semiconductors, and therefore, the DFT + U method extends the functional approach to deal with the self-interacting electron correlations. It combines the high efficiency of GGA and explicates the treatment of correlation with a Hubbard-like model for a subset of states in the system. Thus, GGA + U is strongly suggested to be used to examine the spin-gapless semiconducting behavior of PSGSs and DSGSs. Moreover, the hybrid functional based on a

screened Coulomb potential by Heyd, Scuseria, and Ernzerhof (HSE)[60] accurately describes band gaps and magnetic effects for DSGSs. Thus, HSE06 has been widely used for calculating DSGSs in recently years. In addition, for some DSGS-type materials containing heavy elements, the spin-orbit coupling effect[61] is also taken into account. To exhibit the magnetism of DSGSs, the spin-polarized DFT calculations[62] are used in studies to indicate that the calculations will be performed using different orbitals for different spins. In order to obtain more accurate results, we hope that researchers can calculate the electronic structure of the material by means of GGA-PBE, GGA + U, and HSE06 and then compare results in PSGSs/DSGSs theoretical prediction study in future.

Overall, the DFT calculation has been widely employed in computational materials science due to the fact that it provides us a cheap and powerful tool. Compared to the experimental designing of materials, which consume much time and energy and inevitably causing a waste of experimental resources, DFT calculation does not need any real sample and can be performed even for DSGS materials that have not been prepared yet. Further, with the help of DFT calculation, the experimental researchers can theoretical predict the materials first and then synthesize them on demand. Such a procedure can largely reduce the period of materials design. Moreover, owing to the development of computer technology and theoretical physics and chemistry, the speed and accuracy of DFT calculations have both been largely improved.

Moreover, lots of PSGSs have been prepared in experiment[63] according to the theoretical results, and we hope that the calculations of DSGSs will supervise the experiment and the more DSGSs can be realized in experiment soon.

III. DSGSs AND DHMs

We should point out here that some researchers may neglect the differences in band structures between DSGS and DHM. The band structures of DSGS and DHM are shown in Fig. 1. One can see that the Dirac point of DHM is located above (or possibly below) the Fermi level. The Dirac point of DHM does not intersect with the Fermi level, but it is in its vicinity, as shown in Fig. 1, clearly indicating that this kind of band structure is half-metallic. By contrast, DSGS is essentially defined by the observation that its conducting band and valence band exactly meet each other at the Fermi level (called as the Dirac-like gapless state) in one spin channel. In other words, the DSGS may have a more strict definition in that its Dirac point should intersect the Fermi level rather than simply being located near the Fermi level. We hope that our discussions may give researchers a clearer understanding of both concepts of Dirac materials.

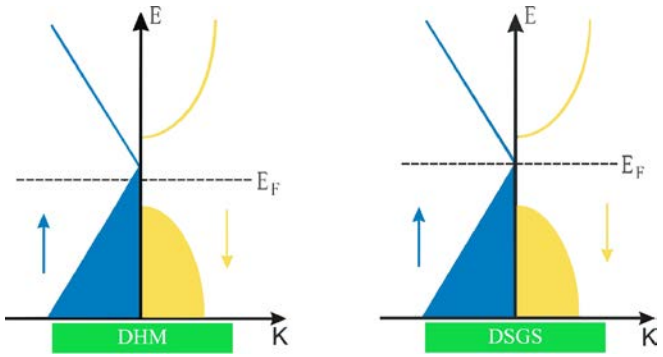

FIG. 1. Band structures of DHM and DSGS. The Dirac point of DSGS is exactly located at the Fermi level, unlike that of DHM. Owing to the intersection of the Dirac point and Fermi level, DSGS possesses the real gapless property rather than half-metallic property in one spin channel.

IV. THE d-STATE TYPE DSGSs

To date, the majority of DSGS members are *d*-state type materials. Usually, for *d*-state type DSGSs, the Dirac states are derived mainly from the *d*-orbitals of the TM atoms, with the *p*-orbitals of MG atoms making only a small contribution. In this case, the *d*-state type DSGS may experience some impact from the localization of *d*-electrons and the relatively larger spin-orbit coupling.

A. Mn-intercalated epitaxial graphene on SiC (0001)

Graphene is well known to possess a series of desirable properties for a number of research fields, but its applications in spintronics are limited owing to its degenerate Dirac states. Mn-intercalated epitaxial graphene, as a DSGS, was theoretically proposed by Li *et al.*[64] in 2015. The homologous lattice model is displayed in Figs. 2(a) and 2(b). In simple terms, the Mn atoms are sandwiched by a graphene monolayer and the SiC (0001) substrate. The changes in the Mn coverage χ (defined as the ratio of one Mn atom to the corresponding surface Si atoms per unit cell) affect the *p*-*d*-orbital hybridization between Mn *d*- and C *p*-orbitals; this can be used to engineer the electronic structure and magnetism of the material. For the same reason, its DSGS state only exists in a given Mn coverage range. By means of first-principles theory, the DSGS state of such system will appear at 1/3 ML $< \chi <$ χ_{max}, while 5/12 ML $<$ χ_{max} $<$ 1/2 ML (1 ML is defined as one Mn atom per surface Si atom). The Dirac state of the material is thus "tunable" by means of such substrate modulations. The above-mentioned behaviors of such a system can be explained in detail by analyzing the Mn-SiC interaction and its quasi-2D inversion symmetry. As a typical example, the band structures and total density of states (DOS) of the $\chi = 5/12$ ML model were calculated by Li *et al.* and are displayed in Fig. 2(c). The majority-spin channel showed a gap of 190 meV, whereas the Dirac cone emerged in a minority-spin channel possessing gapless property. The DOS also demonstrates that the main contribution near the Fermi level is from the Mn atoms, indicating that the Mn-intercalated epitaxial graphene belongs to *d*-state DSGSs. More interestingly, before the theoretical work done by Li *et al.*, in 2012, Gao *et al.* had reported experimental coverage tuning on the basis of Mn intercalated epitaxial graphene on SiC (0001),[65] and the intrinsic Dirac states were confirmed explicitly. In Fig. 2(d), we can clearly see the Dirac point shifting down under the effect of Mn coverage tuning. Meanwhile, the Dirac state vanished when $\chi = 0.6$ ML, in good agreement with the theoretical investigation. Importantly, however, its Dirac state was recovered to the

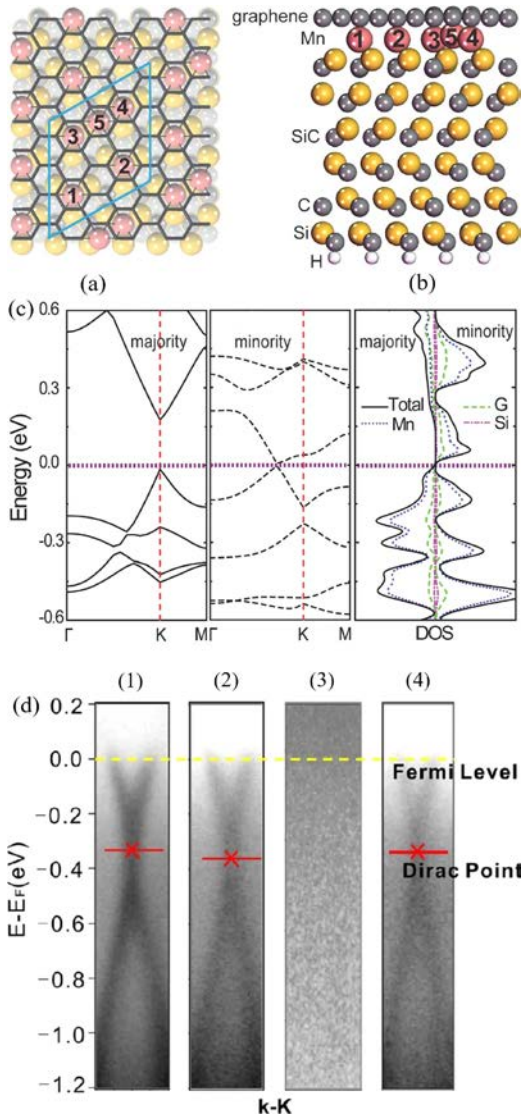

FIG. 2. (a) and (b) Optimized geometric structure of Mn-intercalated epitaxial graphene in the case where $\chi = 5/12$. The numbers (1)–(5) indicate the five different Mn atoms. Mn-3, Mn-4, and Mn-5 form a trimer. (c) Band structure and corresponding DOS of $\chi = 1/3$ML Mn-interacted graphene. Both the majority-spin and the minority-spin channels are displayed. Figures and captions are reproduced with permission from Li *et al.,* Phys. Rev. B **92**(20), 201403 (2015). Copyright 2015 American Physical Society. (d) from left to right: (1), (2), (3), and (4). (1) Band structure of epitaxial graphene with linear dispersion; (2) $\chi = 0.1$ ML interaction; (3) $\chi = 0.6$ML interaction; and (4) recovering graphene band by heating sample 3 up to 1200 °C. Figures and captions are reproduced with permission from Gao *et al.,* ACS Nano **6**(8), 6562–6568 (2012). Copyright 2012 American Chemical Society.

native state (without Mn-intercalation) in parallel with the desorption of Mn when sample (3) [in Fig. 2(d)] was heated to 1200 °C for a short time. The further experimental work is still warranted. In addition, the other physical properties of such systems have not yet been studied in depth. However, the topological phase transition caused by spin-orbit coupling (SOC) can pave the way to achieve the quantum anomalous Hall effect (QAHE).

B. CrO_2/TiO_2 heterostructures

Rutile chromium dioxide (CrO_2) and Co-doped titanium dioxide have been shown to be half-metallic materials.[66–68] Cai *et al.*[69] investigated two types of CrO_2/TiO_2 heterostructures, a superlattice of CrO_2 and TiO_2, and ultrathin films of CrO_2 coupled to a TiO_2 substrate. They considered a series of $(CrO_2)_n/(TiO_2)_m$ thin films and superlattice models with indices (n-m) in their first-principles studies. The crystal structure models and corresponding band structures of the (4–10) superlattice and (5–9) thin film are shown in Figs. 3(a)–3(f). Two symmetric Dirac cones can be seen across the Fermi level along the diagonals of the Brillouin zone (BZ) in Fig. 3(e). For the (5–9) thin film, there are four asymmetric Dirac cones [Fig. 3(f)]. The numerical gaps were calculated to be less than 0.1 meV, that is, vanishingly small. Thus, both systems are confirmed to be DSGSs, and their principal Fermi velocities (v_F) were calculated into the range of 1.00 to 2.20×10^5 m/s. These Dirac states were also shown to be contributed by the 2D CrO_2 layer and dominated by *d*-orbitals of Cr atoms, indicating that both systems belong to the *d*-state type. Moreover, the Dirac points in the above interfacial electronic phases are extraordinary, for the following reasons: (i) they are single-spin Dirac species; and (ii) these Dirac points are field-tunable, i.e., they can be massless or massive, depending on straightforward field alignment. In their article, with consideration of SOC, they can obtain the quantum anomalous Hall phase with Chern number $= \pm 2$ in superlattice at a relatively high temperature. That is, such heterostructures could be used to design ideally dissipation-less digital signal transmission with minimal influence of noise.

C. Two-dimensional metal-organic frameworks (MOFs)

Members of the MOF family are regarded as potential candidates for SGSs in 2D materials.[70] Owing to the success of the molecular building method, MOFs have been widely investigated, allowing their structures and physical properties to be precisely controlled at molecular level.[71–73] Thus, they merit consideration with respect to the design of DSGS materials. Here, we will review some intrinsic Dirac-type MOFs.

1. Two-dimensional $Mn(C_6H_5)_3$ MOFs

Benzene, which is the most common chemical product, may also have potential as a constituent of MOFs and shows some novel spintronic properties. In 2013, Wang *et al.*[74] proposed the possibility of establishing 2D MOFs based on benzene to realize the QAHE. $Mn(C_6H_5)_3$ (TM_n) was built using one Mn atom and three benzene rings, with three-fold rotational symmetry, as shown in Figs. 4(a) and 4(b). It naturally forms a hexagonal lattice. In the absence of SOC, TM_n is ferromagnetic, with a magnetic moment of $4\mu_B$ per unit cell. Its novel band structures are shown in Fig. 4(c), where two Dirac cones can be seen in the spin-down channel crossing the Fermi level, and possessing gapless features. Furthermore, both of two cones are high-symmetric, and the Fermi level exactly located at the Dirac points (K and K'). In the spin-up channel, two similar Dirac cones can be seen below the Fermi level. The projected DOS (PDOS) illustrations reveal that the Dirac states are mainly derived from the *d*-orbitals of Mn,

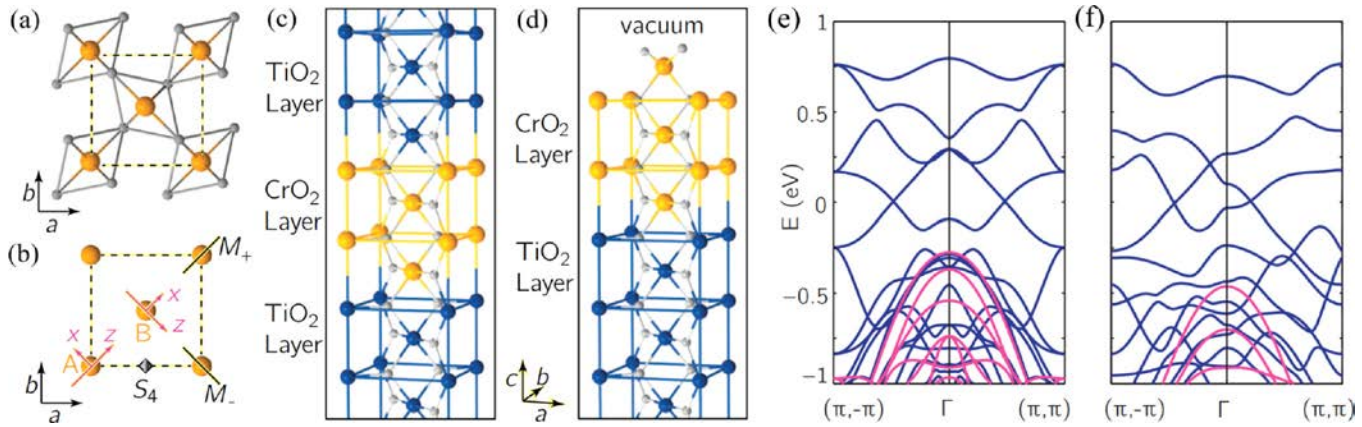

FIG. 3. (a) Rutile structure cleaved along (001) plane. (b) Symmetry and local coordinates of a XO_2 unit cell. (c) The corresponding structure model of superlattice of CrO_2 and TiO_2. (d) The corresponding structure model of thin film of CrO_2 on TiO_2 substrate. Here, *xyz* represent local coordinates and *abc* are global coordinates. Blue, orange, and gray balls represent Ti, Cr, and O, respectively. (e) and (f) Non-relativistic DFT band structure of superlattice and thin film models, respectively. Here, the blue and red bands represent two different spins. Figures and captions are reproduced with permission from Cai *et al.,* Nano Lett. **15**(10), 6434–6439 (2015). Copyright 2015 American Chemical Society.

with only a small contribution from the *p*-orbitals of C atoms [Fig. 4(d)]. Thus, TM_n was confirmed to be a *d*-state DSGS.

The main goal of Wang *et al.* was searching for a platform with which to realize the QAH state. Thus, they did not analyze any other properties of TM_n in detail. To determine its topological non-triviality, they investigated the relevant influences, taking SOC into account. For this reason, the gaps between the two pairs of Dirac cones were opened up to the value of 9.5 meV in the spin-down channel, as can be seen clearly in Fig. 5(a). As a topological non-trivial material, TM_n was shown to be a suitable candidate to realize QAHE, owing to the gap between the Dirac cones and the lifted degenerated points possessing a nonzero Chern number (*C*), and exhibiting the gapless chiral edge state within the Dirac gap, as shown in Fig. 5(b).

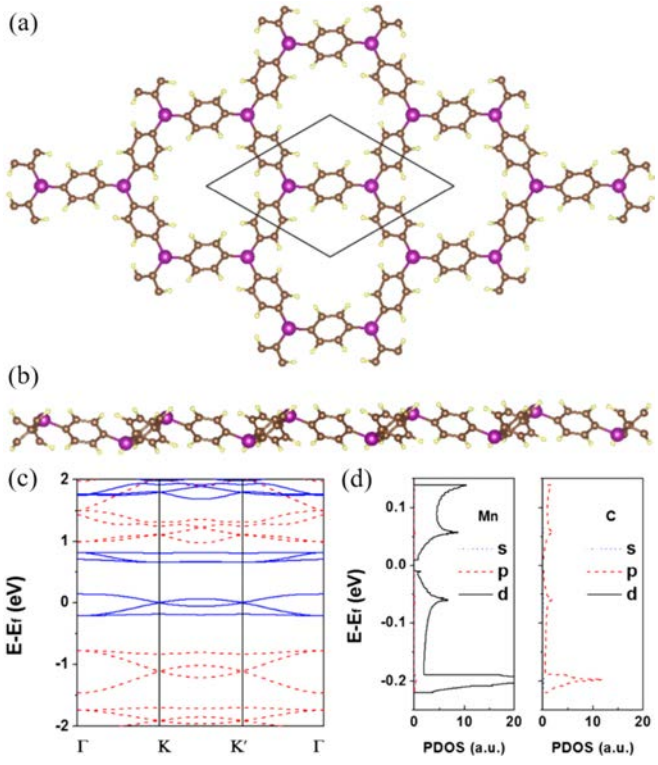

FIG. 4. (a) and (b) Top and side views of optimized geometric lattice structure of TM_n. (c) Spin-resolved band structure of $Mn(C_6H_5)_3$. The red and blue lines represent spin-up and spin-down channels, respectively. (d) PDOS of Dirac states near the Fermi level. Figures are reproduced with permission from Wang *et al.,* Phys. Rev. Lett. **110**(19), 196801 (2013). Copyright 2013 American Physical Society.

2. Two-dimensional $Ni_2C_{18}H_{12}$ and $Co_2C_{18}H_{12}$ MOFs

Two other species of 2D MOFs have been designed based on benzene, $Ni_2C_{18}H_{12}$ and $Co_2C_{18}H_{12}$, by Ma *et al.*[75] In both materials, every two Ni or Co atoms bond with three benzene rings, as shown in Fig. 6. In the optimized geometric structure, both kinds of lattices ($Ni_2C_{18}H_{12}$ and $Co_2C_{18}H_{12}$) are buckled. The Ni system appears to be only slightly buckled, while the Co system possesses two favorable configurations, low-buckled (LB) and high-buckled (HB). Their electronic and magnetic properties were investigated in detail by Ma *et al.* using first-principles calculations. The results showed that the HB $Co_2C_{18}H_{12}$ was spin-unpolarized, whereas the other two systems (LB $Co_2C_{18}H_{12}$ and $Ni_2C_{18}H_{12}$) possessed spin-polarization properties. Furthermore, both $Ni_2C_{18}H_{12}$ and LB $Co_2C_{18}H_{12}$ systems displayed robust magnetism caused by large energy differences between the corresponding FM states and non-ferromagnetic (NM) states. Ma *et al.* also predicted that, via geometric structure modulation, $Ni_2C_{18}H_{12}$ systems could have tunable magnetism similar to that of $Co_2C_{18}H_{12}$ systems. Therefore, $Ni_2C_{18}H_{12}$ may be also used for magnetic storage.

The spin-resolved band structures of LB $Co_2C_{18}H_{12}$ and $Ni_2C_{18}H_{12}$ without SOC are shown in Fig. 6. In the spin-up channel, the intersections of Dirac points and Fermi levels in both systems are clearly visible. In the spin-down channel, the semiconducting gaps can also be seen. Therefore, mainly owing to the contribution from TM *d*-orbitals near the Fermi level, as confirmed by DOS analysis, both of the MOFs were shown to be *d*-state DSGSs. In contrast, band structure calculations showed that the HB $Co_2C_{18}H_{12}$ possessed a similar Dirac state, comparable to those of LB type and Ni system, above the Fermi level at about 1.22 eV, as shown in Fig. 6.

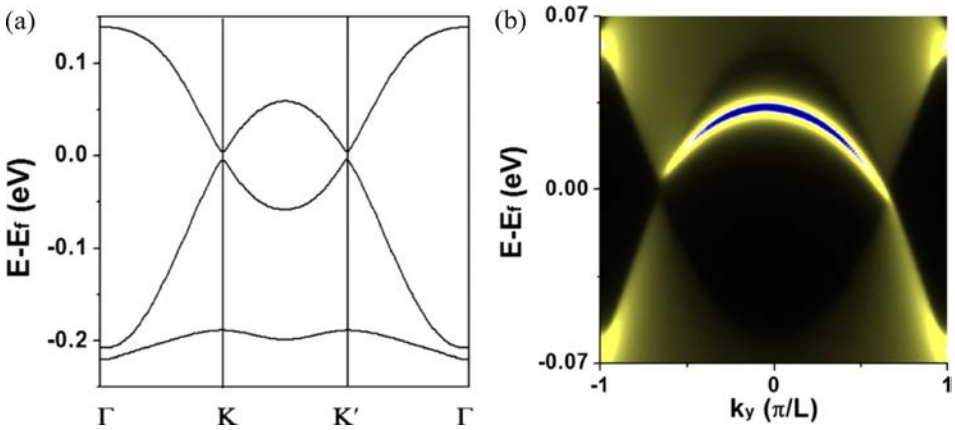

FIG. 5. (a) Small gaps between two Dirac cones occurring when the SOC is considered. (b) Semi-infinite edge state within the Dirac gaps of $Mn(C_6H_5)_3$. Figures are reproduced with permission from Wang *et al.*, Phys. Rev. Lett. **110**(19), 196801 (2013). Copyright 2013 American Physical Society.

The Dirac point of the HB type may be shifted down by some possible methods, such as doping, to achieve the true DSGS state. This indicates that these materials could be used to realize massless fermions and dissipation-less properties near the Fermi level, owing to their DSGS behaviors. To further examine the possibility of achieving QAH states, Ma *et al*. found that the gap could be opened by considering SOC. Thus, there is potential for the QAHE and quantum spin Hall effect (QSHE) to be realized in such materials in future work. However, the dynamical and thermal stabilities of these materials have not yet been computed, and we hope that further investigation into these materials can be done not only in theory but also experimentally.

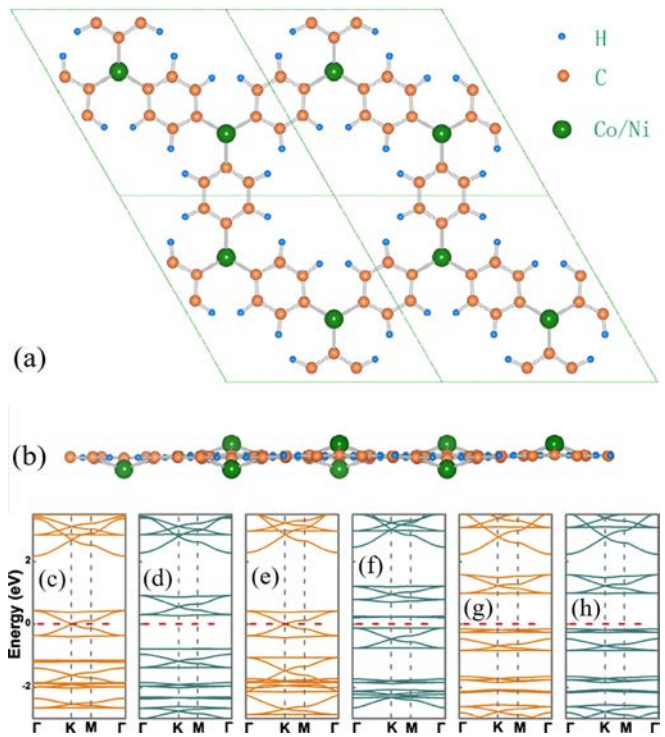

FIG. 6. (a) and (b) Optimized geometric structures of $Ni_2C_{18}H_{12}$ and $Co_2C_{18}H_{12}$. Dashed lines represent the unit cell. (c) and (d) Band structures of $Ni_2C_{18}H_{12}$ in two spin channels. (e) and (f) Band structures of LB $Co_2C_{18}H_{12}$ in two spin channels. (g) and (h) Band structures of HB $Co_2C_{18}H_{12}$ in two spin channels. Orange and dark cyan lines present the spin-up and spin-down channels, respectively. Figures and captions are reproduced with permission from Ma *et al.*, Carbon **73**, 382–388 (2014). Copyright 2014 Elsevier Publications.

3. Two-dimensional $Ni_2C_{24}S_6H_{12}$ MOFs

As in the case of graphene, some materials based on thiophene possess notable advantages, e.g., light weight, high carrier mobility, and tunable electronic properties; they also have some applications in conducting polymers.[76] Owing to the above properties, it is reasonable to consider thiophene as a potential material for use in a 2D MOF system. By means of first-principles calculations, Lin *et al*.[77] proposed a new *d*-state DSGS, called 2D $Ni_2C_{24}S_6H_{12}$ MOF, in 2016.

Lin *et al*. first established a large 2×2 supercell (see Fig. 7) containing 176 atoms to carry out *ab initio* molecular dynamics (AIMD) simulations, as this kind of system is dynamically stable at room temperature. They also defined the formation energy of the framework through a hypothetic reaction, showing that this MOF may have synthetic plausibility in thermodynamics. For experimentally realizing the DSGS state in 2D materials, these results may provide a suitable starting point for other researchers to build on in future work. Figure 7 also shows the spin-resolved band structures of this MOF system in the absence of SOC. Clearly, the conduction band and the valence band truly meet at the Fermi level in the spin-up channel, with a linear energy dispersion. In the spin-down channel, a semiconducting gap of 1.29 eV can be seen. Thus, this system is confirmed to be a DSGS. Interestingly, the Dirac type band structures were sandwiched by two flat bands, respectively, and the Dirac type bands and flat bands were degenerated. In contrast to kagome bands, which consist of two Dirac type bands and one flat band, this kind of band structure in $Ni_2C_{24}S_6H_{12}$ comprises two Dirac bands and two flat bands. On the one hand, kagome bands indeed contribute to the topological nontriviality of a homologous kagome lattice system. On the other hand, they connect the profile of the four bands in $Ni_2C_{24}S_6H_{12}$ with a ruby lattice, which had been proposed for achieving the fractional quantum Hall effect (FQHE),[78] but the $Ni_2C_{24}S_6H_{12}$ was fully spin-polarized rather than spin-unpolarized. However, no further study was performed on these attractive potential features that are connected to other important research topics in the condensed matter physics.

The v_F was also calculated, and it had a value of 1.25×10^5 m/s. The stability of the ferromagnetism was

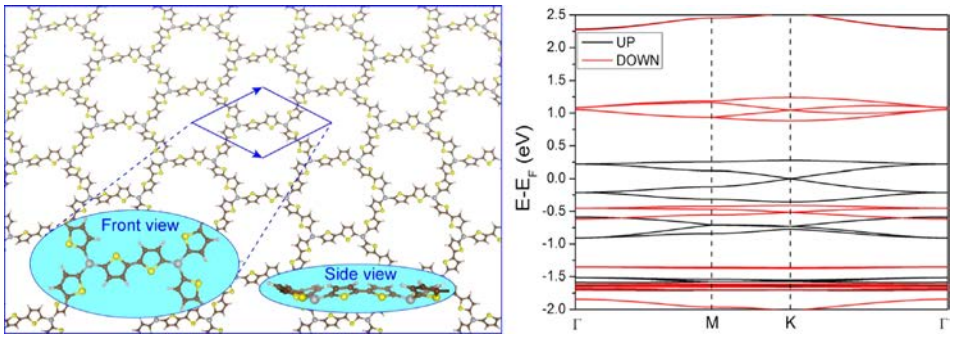

FIG. 7. Left: Schematic representation of the atomic configuration of the $Ni_2C_{24}S_6H_{12}$ framework and Right: Spin-resolved band structure of $Ni_2C_{24}S_6H_{12}$ MOFs without SOC. The energy at the Fermi level was set to zero. Figures are reproduced with permission from Lin *et al.*, Phys. Chem. Chem. Phys. **18**(11), 8059–8064 (2016). Copyright 2016 Royal Society of Chemistry.

confirmed by Monte Carlo (MC) simulations with an Ising model carried out on a 50×50 supercell. As shown in Fig. 8, the magnetic moment per unit cell decreased from almost $1.6\,\mu_B$ to $0.0\,\mu_B$ in the temperature range of 600–630 K. Taking C_V into account, the T_C was considered to be about 630 K and its ferromagnetic transition was a second-order phase transition. Furthermore, this system could be transformed to be a Chern insulator and realize the QAHE at a suitable temperature, while exerting the SOC. Overall, $Ni_2C_{24}S_6H_{12}$ MOFs have great potential in spintronic devices and other electronic applications.

4. Two-dimensional $Mn_2C_6S_{12}$ MOFs

In 2017, Wang *et al.*[79] proposed a MOF called $Mn_2C_6S_{12}$ using first-principles calculations. They demonstrated that the $Mn_2C_6S_{12}$ lattice possessed intrinsic spin-polarization. Its honeycomb lattice structure is shown in Fig. 9(a), and the dynamic stability was confirmed by the phonon spectrum shown in Fig. 9(b). The spin-resolved band structure is shown in Fig. 9(c). The gap in the spin-down channel is about 1.53 eV, and the Dirac point in the spin-up channel intersects with the Fermi level. Owing mainly to contributions from *d*-orbitals of Mn atoms, the Dirac state was confirmed to be of the *d*-state type. These characteristics were also revealed by isosurface Kohn-Sham wave functions in Fig. 9(d). The v_F of electrons and holes was calculated to be as low as about 0.30×10^5 m/s, caused by the long lattice constant and large voids in the porous framework; indeed, its value was almost the of same order as the electron saturation velocity in silicon crystals ($\sim 10^5$ m/s), implying high electron mobility and potential applications of the material in spin-filter devices. Furthermore, Wang *et al.* confirmed the stability of FM state using MC simulations within Ising model. An extremely high Curie temperature (T_C) of about 1280 K was observed, and the ferromagnetic transition was a second-order phase transition, as shown in Fig. 10(a). Thus, there is evidence that the ferromagnetism of this material is robust enough at room temperature, possibly making it an important candidate for future spintronic devices. With consideration of SOC, the gap opened between Dirac cones will lead to QAHE. The degenerate two spin channels lifted by SOC result in two type-I gaps, i.e., $\Delta 1 = 7.79$ meV and $\Delta 2 = 15.10$ meV, as shown in Fig. 10(b). Under a small gate voltage, the Fermi level can be moved into gap $\Delta 1$ making $Mn_2C_6S_{12}$ lattice behave as a Chern topological insulator. To move the Fermi level into gap $\Delta 2$, $Mn_2C_6S_{12}$ lattice will behave as a Chern half-metal. The SOC can also lead to two type-II gaps ($\Delta 3$ and $\Delta 4$) arising from the intraspin interaction. This is the first report on the coexistence of type-I and type-II gaps in 2D materials. Also, the Chern insulator and Chern half-metal behaviors can be obtained separately in $Mn_2C_6S_{12}$ lattice by moving the Fermi level into two type-II gaps. Moreover, to confirm the topologically non-trivial nature of the $Mn_2C_6S_{12}$, the calculation of *C* was carried out by Wang *et al.* The calculated anomalous Hall conductivity curve is shown in Fig. 10(c). The calculated *C* of SOC gaps $\Delta 1$ and $\Delta 3$ possess an integer value of -1, while that of SOC gaps $\Delta 2$ and $\Delta 4$ possessing slightly deviated values of ± 1. Wang *et al.* also calculated the local density of states of edge, as shown in Fig. 10(d). One can see that the bulk states are connected by the topologically non-trivial edge states, which can be found in Chern insulator. Further, the separation between bulk SOC bandgaps and other bands prove the feasibility of realizing QAHE at room temperature.

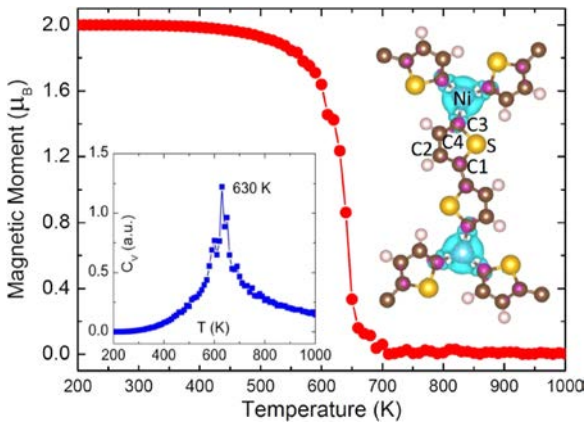

FIG. 8. Evolution of average magnetic moments per unit cell as a function of temperature obtained from a Monte Carlo simulation within an Ising model. The variation of heat capacity (C_V) is plotted in the inset. The spatial distribution of the spin-polarized electron density $\Delta\rho$ calculated from the difference between the electron densities of the two spin channels ($\Delta\rho = \rho_\uparrow - \rho_\downarrow$) is shown in the top right panel. Figures and captions are reproduced with permission from Lin *et al.*, Phys. Chem. Chem. Phys. **18**(11), 8059–8064 (2016). Copyright 2016 Royal Society of Chemistry.

D. Transition metal halides

Very recently, the transition metal (TM) halides, as potential new DSGSs, have become a focus of increasing attention owing to their DSGS (even multiple) band structures, high stability, and, rarely, novel electronic properties. Most importantly, there is the possibility of synthesis of such

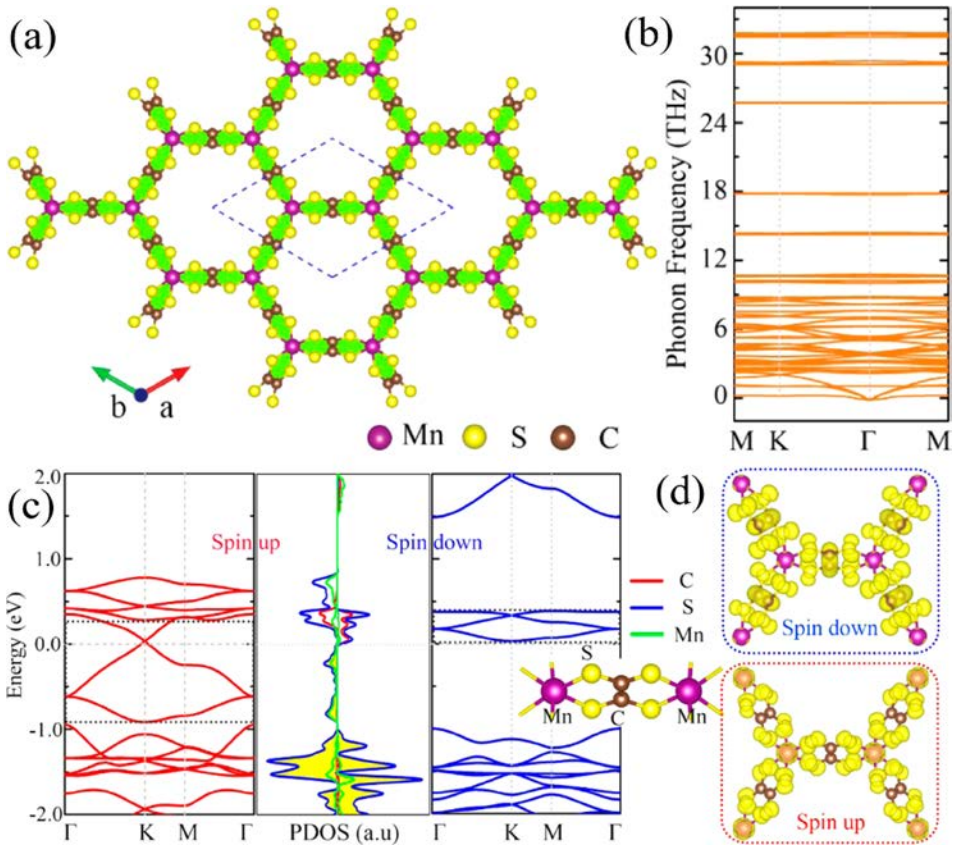

FIG. 9. (a) $Mn_2C_6S_{12}$ MOFs lattice designed into a honeycomb lattice. (b) The phonon spectrum shows no imaginary frequency, indicating its synthetic determinacy in the laboratory. (c) Band structure and PDOS of $Mn_2C_6S_{12}$ MOFs. The energy at the Fermi level was set to zero. (d) Isosurfaces of the Kohn-Sham corresponding to the states (indicated by the black dotted region) nearest to the Fermi level. Figures are reproduced with permission from Wang *et al.*, J. Phys. Chem. Lett. **8**(16), 3770–3775 (2017). Copyright 2017 American Physical Society.

materials. These new reports of TM halides will be discussed below.

1. Vanadium trihalide monolayer

A layered configuration usually endows an ordinary material with some novel properties, especially the monolayer configuration. In 2016, He *et al.*[80] established VCl_3 and VI_3 monolayers (illustrated in Fig. 11) and systematically investigated their various characteristics using first-principles calculations. As expected, both materials were Dirac HMs, and their high carrier mobility in one spin-channel implied that they have potential applications in spintronics. Band structures and total DOS illustrations (as shown in Fig. 12) revealed that both VCl_3 and VI_3 possess linear energy dispersions, with their Dirac points located above the Fermi level (approximately 20 and 106 meV above the Fermi level, respectively). The calculated v_F were approximately 1.60×10^5 m/s and 1.00×10^5 m/s, for the VCl_3 and the VI_3 monolayers, respectively, both of which are markedly higher than those of many other Dirac-type materials. Upon investigating the PDOS illustrations, they found the contributions for the Dirac states from the *d*-orbitals of V atoms, but none from the *p*-orbitals of Cl or I atoms. Consequently, both monolayers belong to the *d*-state type. The T_C values were also computed using MC simulations. Corresponding analysis spectrum showed that the second-order phase transitions occurred at 80 and 98 K, respectively. Therefore, combining analyzing the evolution of homologous C_V values, the values of T_C were confirmed to be 80 and 98 K, respectively. These T_C values were relatively low compared with those of other Dirac type materials. Thus, He *et al.* used doping to tune the T_C values in order to obtain more stable ferromagnetism in the VCl_3 and VI_3 monolayers.

Notably, the Dirac points were shifted down as a result of doping, and exactly intersected with the Fermi level when electron doping levels of 0.1 and 0.7 per unit cell, respectively, were used, as shown in Fig. 12. The spin exchange parameters were also calculated as J_n. Under doping

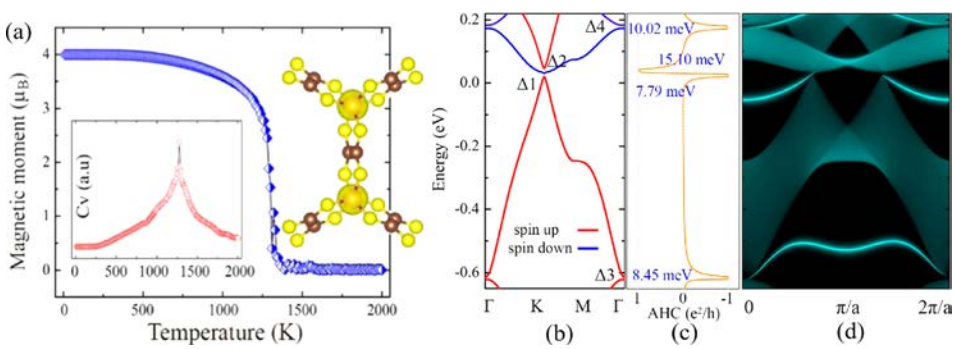

FIG. 10. (a) Average magnetic moment per Mn atom shown as a function of temperature. Corresponding total DOS and temperature-dependent heat capacity are also shown. (b) Band structures of the $Mn_2C_6S_{12}$ lattice with SOC. (c) Calculated AHC and (d) semi-infinite edge states according to MLWFs. Figures are reproduced with permission from Wang *et al.*, J. Phys. Chem. Lett. **8**(16), 3770–3775 (2017). Copyright 2017 American Physical Society.

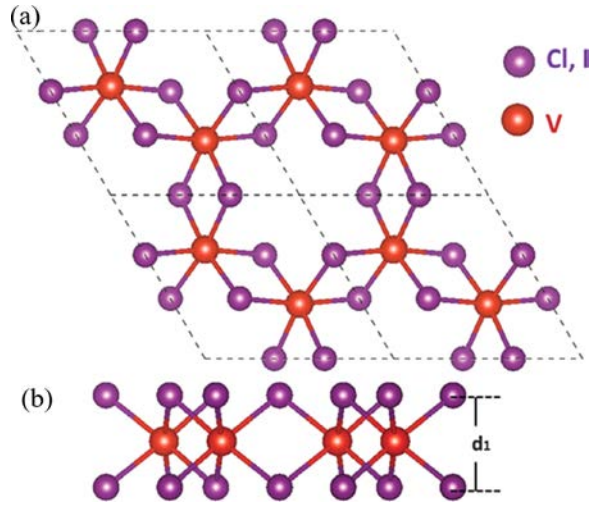

FIG. 11. The top (a) and side (b) views of the VX_3 (X = Cl, I) monolayer. Figures are reproduced with permission from He *et al*., J. Mater. Chem. C **4**(13), 2518–2526 (2016). Copyright 2016 Royal Society of Chemistry.

conditions, the Dirac half-metallic states transformed to DSGS states, suggesting that this could be an effective method to tune the band structures of previously identified DHMs to obtain a series of possible DSGSs. Furthermore, He *et al*. carried out computations of cleavage energies, resulting in values of 0.11 and 0.18 J/m^2 for VCl_3 and VI_3, respectively. It also proved possible to exfoliate layers from the bulk phase. Given that the bulk phase VCl_3 and VI_3 have been widely investigated for so long, researchers may now have enough confidence to synthesize both monolayers in experiments.

2. Nickel chloride monolayer

Following on from their previous work,[80] He *et al*.[81] proposed the $NiCl_3$ monolayer as a new candidate for DSGSs using first-principles calculations. The band structures were calculated based on two different computation methods, PBE and HSE06; the results are shown in Fig. 13. Both spin-up channels show linear energy dispersions, with zero gap between the conduction band and the valence band, indicating Dirac spin-gapless states. On the other hand, there were 1.22 eV and 4.09 eV bandgaps in the spin-down channels, respectively. As in the case of the vanadium trihalides, the $NiCl_3$ monolayer was confirmed to be the *d*-state type, according to the PDOS spectrum. Its v_F was high compared with that of other *d*-state DSGSs, with a value of 4.00×10^5 m/s obtained with the HSE06 method, approaching half that of natural graphene (8.50×10^5m/s).[82] Some further investigation was carried out to confirm the stability of the material, including calculation of its 2D Young's modulus (25 N/m) and confirmation of the dynamic stability by AIMD simulation. The AIMD simulation also demonstrated that the structure and the energy of the $NiCl_3$ monolayer were nearly unchanged at 500 K, indicating robust thermal stability at room temperature. Furthermore, the magnetic state was steady owing to an average $2\mu_B$ magnetic moment per unit cell. The T_C was also estimated on the basis of Weiss molecular field theory and MC simulations to be about 400 K, which is high enough to satisfy the conditions of QAHE.

The gaps between Dirac cones will be larger in *d*-state type $NiCl_3$ monolayer than in those in *p*-state DSGS with SOC, and the time-reversal symmetry will be broken. With consideration of SOC, the band structures of $NiCl_3$ monolayer are also shown in Fig. 13. Thus, $NiCl_3$ monolayer, as a typical *d*-state DSGS, is an ideal platform from which to realize QAHE at up to 280 K, and can also be transformed to be a Chern insulator. Confirming this potential of the $NiCl_3$ monolayer, integrating the Berry curve across the entire BZ revealed a *C* value of -1 with a non-trivial topological state.

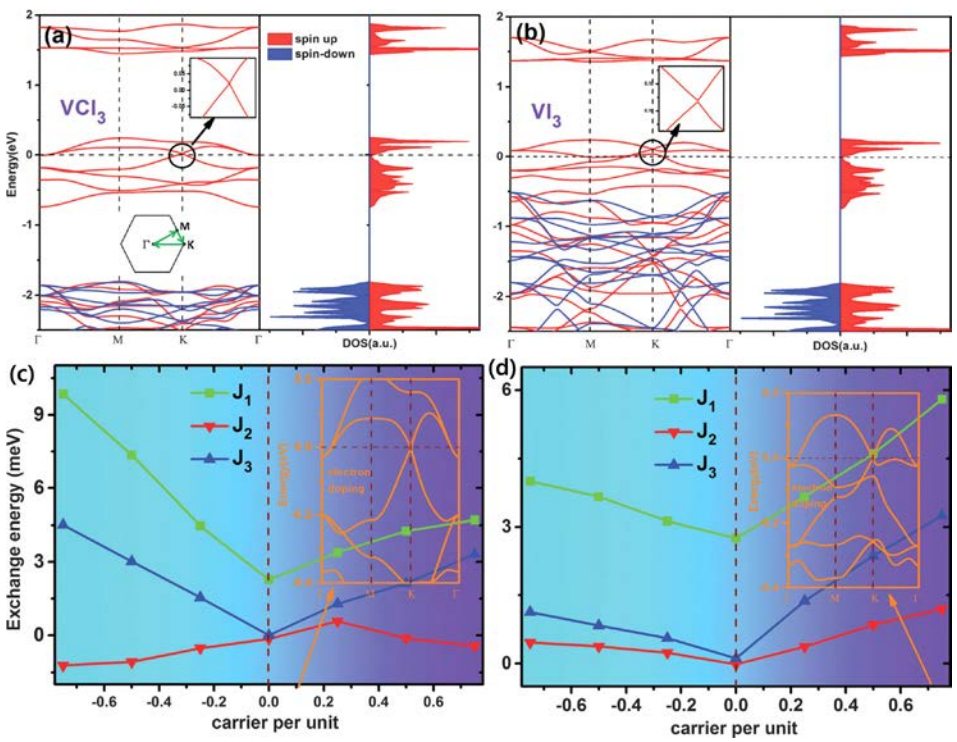

FIG. 12. (a) and (b) Band structures and total DOS for VCl_3 and VI_3, respectively. (c) and (d) Spin-exchange parameters as a function of carrier concentration per unit for VCl_3 and VI_3, respectively. The band structures for electron doping of 0.1 and 0.7 are displayed in the right upper right inset for VCl_3 and VI_3, respectively. The energy of the Fermi level was set to zero in all cases. Figures and captions are reproduced with permission from He *et al*., J. Mater. Chem. C **4**(13), 2518–2526 (2016). Copyright 2016 Royal Society of Chemistry.

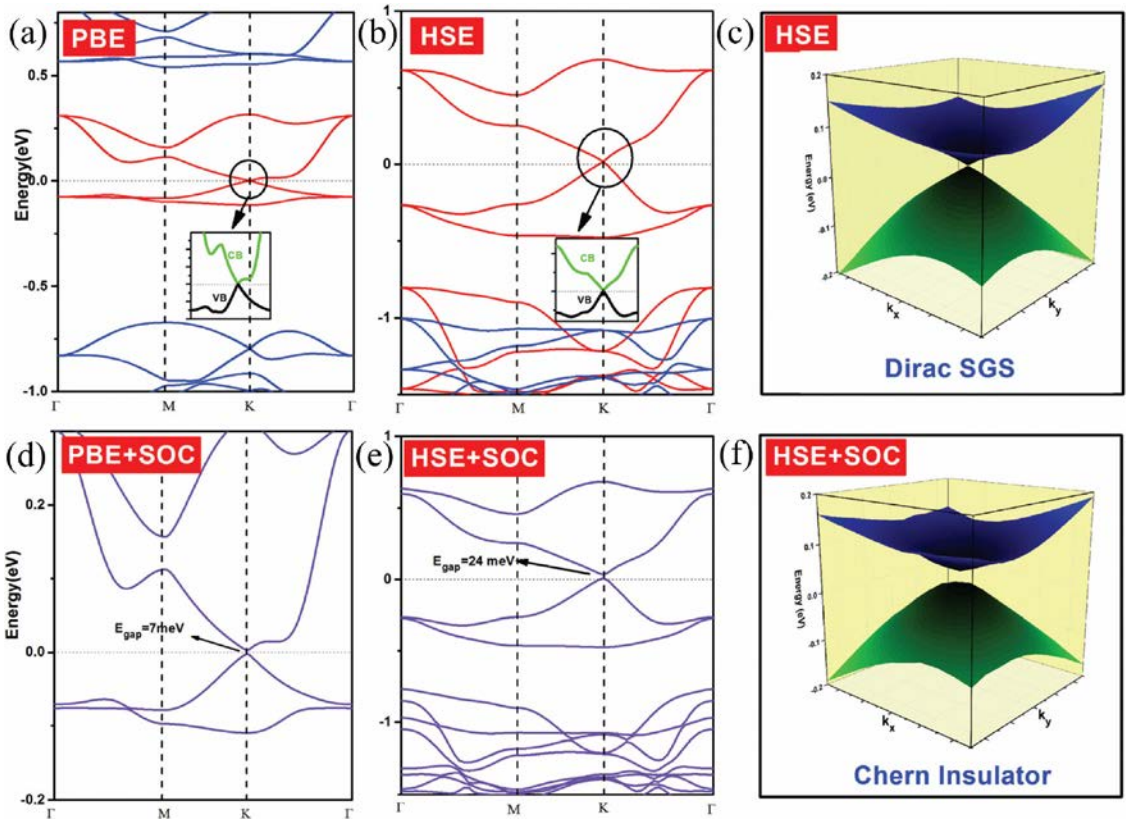

FIG. 13. (a) and (b) Band structures of $NiCl_3$ monolayer without SOC calculated at the PBE and HSE06 levels. The 3D band structures around the Fermi level of $NiCl_3$ monolayer obtained without (c) and with (f) SOC. (d) and (e) The band structures of $NiCl_3$ monolayer with SOC calculated at the PBE and HSE06 levels. The energy of Fermi level was set to zero in these cases. Figures are reproduced with permission from He *et al.*, Nanoscale **9**, 2246 (2017). Copyright 2017 Royal Society of Chemistry.

Specific distribution of Berry curvature in momentum space is displayed in Fig. 14(a). As expected from the non-zero C, when Fermi level is sandwiched by spin-up Dirac cones in the insulating gap, the anomalous Hall conductivity curve shows a quantized charge plateau, as shown in Fig. 14(b). The QAH state will lead to a topologically chiral edge states, to investigate it can reveal the topological non-triviality of $NiCl_3$ monolayer more clearly. Hence, He *et al.* calculated the edge states of $NiCl_3$ monolayer with zigzag and armchair insulator using Green's functions based on Wannier functions obtained from PBE calculations. In Fig. 14, one can see that only one chiral edge state appearing is consistent with the obtained C value of -1. Thus, the topological non-triviality of such system is confirmed. Unfortunately, to investigate the Berry phase and edge states in Fig. 14, the $NiCl_3$ monolayer did not possess an observable valley-polarized edge state, meaning

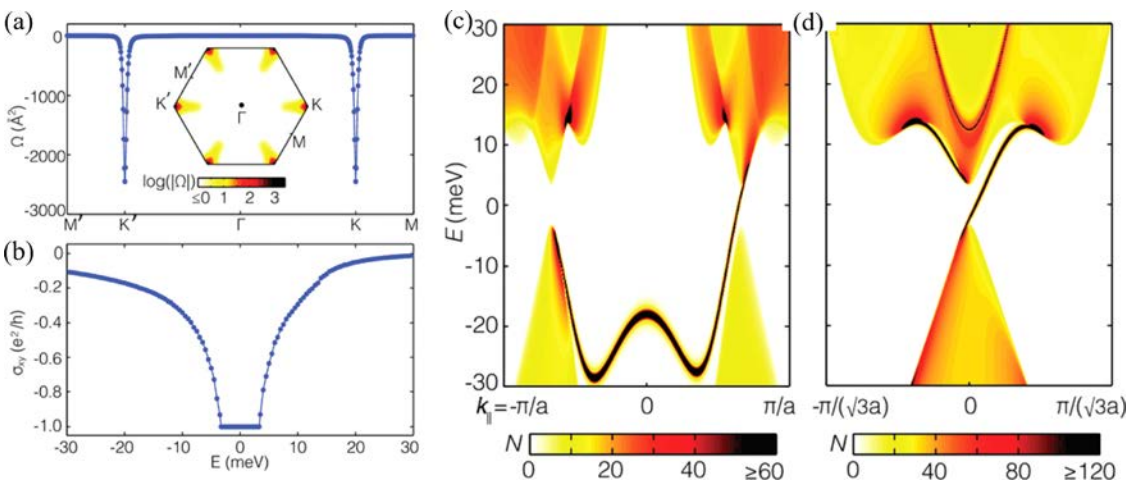

FIG. 14. (a) The distribution of the Berry curvature in momentum space for $NiCl_3$. (b) Anomalous Hall conductivity when the Fermi level is shifted from its original Fermi level. Calculated local density of states of edge states for zigzag (c) and armchair (d) insulator. Figures are reproduced with permission from He *et al.*, Nanoscale **9**, 2246 (2017). Copyright 2017 Royal Society of Chemistry.

that it would not be a suitable alternative material for valleytronic applications. However, as He *et al*. point out, the potential of $TMCl_3$ materials in valleytronics, based on their considerable Rashba SOC, should not be neglected.

3. Manganese halides

This may be the most novel Dirac material family to be discovered recently. As we know, in the past, no true 2D DSGSs had been synthesized in experiment; this is the first predicted 3D bulk materials up to now, it would greatly advance the development of spintronics. Interestingly, already prepared MnF_3 had been identified and investigated by chemists for a long time,[83–86] but there had been no theoretical studies of its electronic band structure. In 2017, Jiao *et al*.[87] demonstrated the DSGS features of MnF_3 by means of first-principles calculations and predicted a series of novel properties. This work focused on a phase of MnF_3 (also called β-MnF_4) that had been synthesized in experiments for many years, i.e., its hexagonal bulk structure (space group, R-3c, No.167), corresponding illustration is shown in Fig. 15(a). This kind of structure was missing from studies of electronics in the past. Moreover, all of the DSGSs that have been predicted were studied based on layered structures rather than bulk phase. This is the first time that the DSGS state was demonstrated to exist in bulk materials by means of first-principles calculations, and more importantly, the fact of synthesis of MnF_3 remind researchers its DSGS state is desire to be confirmed in experiment. Based on investigation of different magnetic configurations, the FM state of MnF_3 was shown to be energetically favorable compared with the antiferromagnetic (AFM) state and NM state. MnF_3 may also possess a significant magnetism, according to analysis. Its three-dimensional magnetic charge density spectrum is displayed in

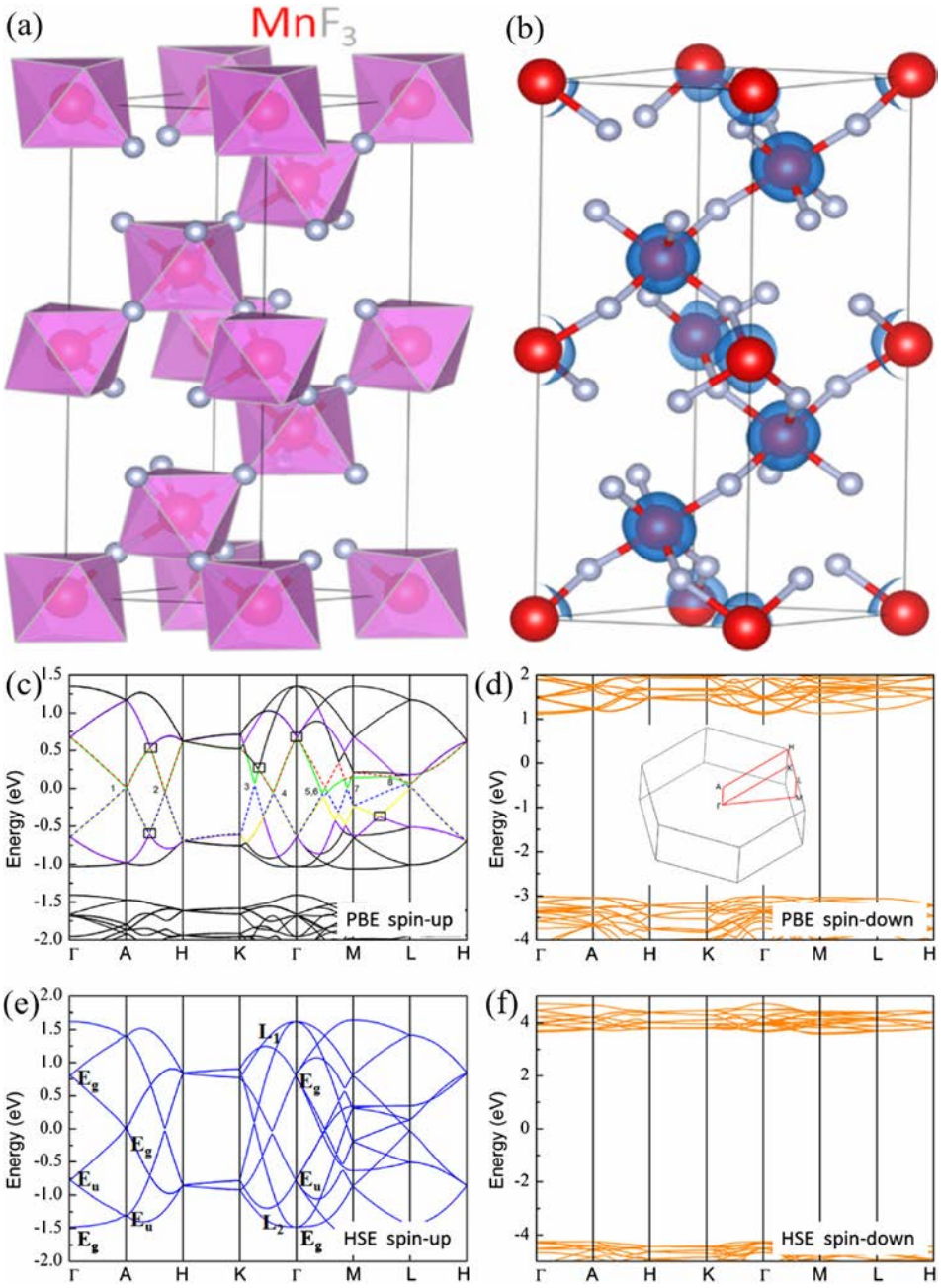

FIG. 15. (a) The crystal structure model of MnF_3. (b) Three-dimensional magnetic charge density of MnF_3. Red, silver, and blue balls represent manganese, fluorine, and magnetic density, respectively. (c)-(f) Band structures in two spin channels of MnF_3 without SOC calculated at the PBE and HSE06 levels. The inset of (d) displays the corresponding Brillouin zone. The energies of Fermi levels for all illustrations are set to zero. Figures are reproduced with permission from Jiao *et al*., Phys. Rev. Lett. **119**(1), 016403 (2017). Copyright 2017 American Physical Society.

Fig. 15(b). In contrast to the single Dirac cone in other DSGSs, multiple Dirac cones were found for MnF_3 by the PBE method, as shown in Figs. 15(c) and 15(e). A total of eight spin-polarized Dirac cones, located at or around the Fermi level without SOC, can be seen in the spin-up channel. Notably, there are both degenerate cones and non-degenerate cones existing simultaneously. In spin-down channel, a semiconducting 4.1 eV gap can be observed. Owing to Pauli repulsion, these Dirac cones have very small gaps, in the range of 1.4–33.8 meV. On the other hand, when the SOC was exerted, the band structure was not significantly altered. Thus, long spin coherence transport can be realized in MnF_3. Interestingly, the results from both the PBE and the HSE06 method showed substantial energy differences between spin-up and spin-down channels, which had not previously been reported. The v_F values of the eight cones ranged from 1.79×10^5 m/s to 3.96×10^5 m/s. Overall, these results indicate that MnF_3 could be the most promising candidate for applications in high-efficiency spin transport. Also, we should point out that the experimental realizations of this novel DSGS states at both low temperature and room temperature are imminent.

Not only did MnF_3 possess an excellent 2D band structure but also displayed the new type of 3D band structure plots (Fig. 16), with two rings of Dirac nodes in the M-K-Γ plane of the BZ. If the symmetry effect is considered, the additional Dirac ring will be present in the A-H-L plane of the BZ. Such kind of Dirac rings is totally different from the other two types of Dirac rings, i.e., countable Dirac cones isolated in the BZ[88] and continuous Dirac cones that form a ring of Dirac nodes[89] or a Dirac loop. As Jiao *et al.* proposed, a more intensive linear response will be implemented in such a system. Owing to the contributions of its multiple Dirac channels, it may possess an extremely high efficiency of carrier transport at the Fermi level. Furthermore, a high carrier mobility can also be found below the Fermi level, as a Dirac ring exists. Thus, the transport properties of MnF_3 deserve to be widely studied. Regrettably, Jiao *et al.* did not carry out the further research on the other features of these novel multiple cones. However, to confirm the stability of the linear band structures in the lattice, they subjected the material to pressures up to 6×10^9 Pa. Unexpectedly, for all the Dirac cones, there was only a slight influence on the cone slopes under such high pressures, indicating the high robustness of MnF_3.

They also carried out some rough calculations to investigate the band structures of CoF_3, FeF_3, and CrF_3. As expected, all three compounds possessed similarly spin-polarized multiple Dirac cones, but the cones were shifted upwards with respect to the Fermi level, comparable to those of MnF_3. These results provide insights which may help researchers to discover more excellent electronic properties in other TM fluorides.

Further research was carried out by Sun *et al.*[90] in 2018, expanding the studies of manganese fluorides[87] from the bulk phase to layered materials. They also computed the corresponding properties of other layered manganese halides, including $MnCl_3$, $MnBr_3$, and MnI_3, using the PBE + U, HSE06, and DFT + U methods. Similarly, ideal DSGS states (Fig. 17) were found in these materials, which were all dynamically and thermally stable, as confirmed by phonon spectra and Born-Oppenheimer molecular dynamics simulations. Combined with the reports by He *et al.*,[80,81] these results strongly suggest that the TM halides should be further investigated owing to their novel physical properties.

V. THE p-STATE-TYPE DSGSs

Most of the *p*-state DSGSs are composed of main group (MG) atoms and are usually found in 2D monolayers. Similarly, the Dirac states of *p*-state-type DSGSs are mainly derived from the *p*-orbitals of MG atoms. However, there are some exceptions to these rules. Here, we will introduce a series of *p*-state DSGSs.

A. Graphitic carbon nitrides

Carbon nitrides have been widely investigated over the past hundred years.[91–97] With the development of topological non-trivial materials, especially graphitic materials, members of this family restarted to receive increasing attention, as their honeycomb-type molecular configurations indicated their potential to be built into graphitic 2D structures. In 2014, the pioneering work that predicted *p*-state DSGSs was reported by Zhang *et al.*[98] In general, most 2D graphitic materials with highly structural symmetries have been built as honeycomb lattice structures. Based on this knowledge, two kinds of graphitic carbon nitride frameworks were built,

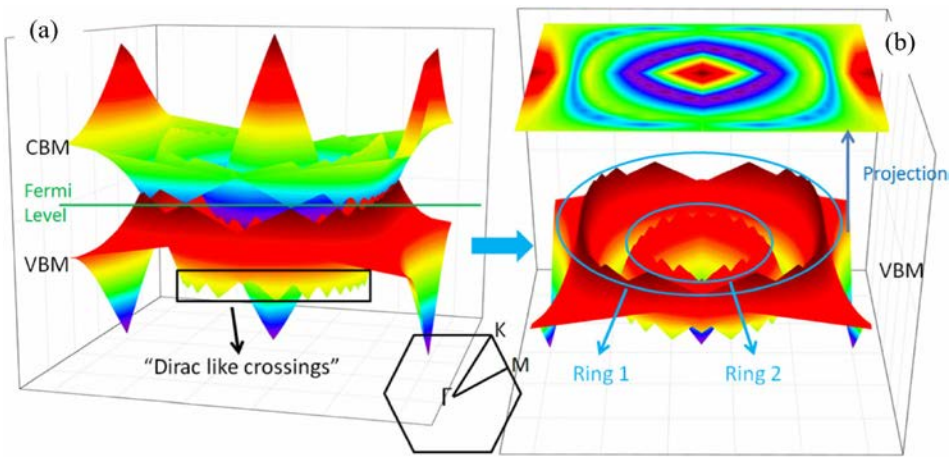

FIG. 16. (a) 3D band structure of MnF_3 in the M-K-Γ plane. (b) 3D band view of VBM and its corresponding projection. The Dirac rings are labeled by blue circles. The corresponding Brillouin zone is presented in the inset. The energies of the Fermi level were set to zero. Figures are reproduced with permission from Jiao *et al.*, Phys. Rev. Lett. **119**(1), 016403 (2017). Copyright 2017 American Physical Society.

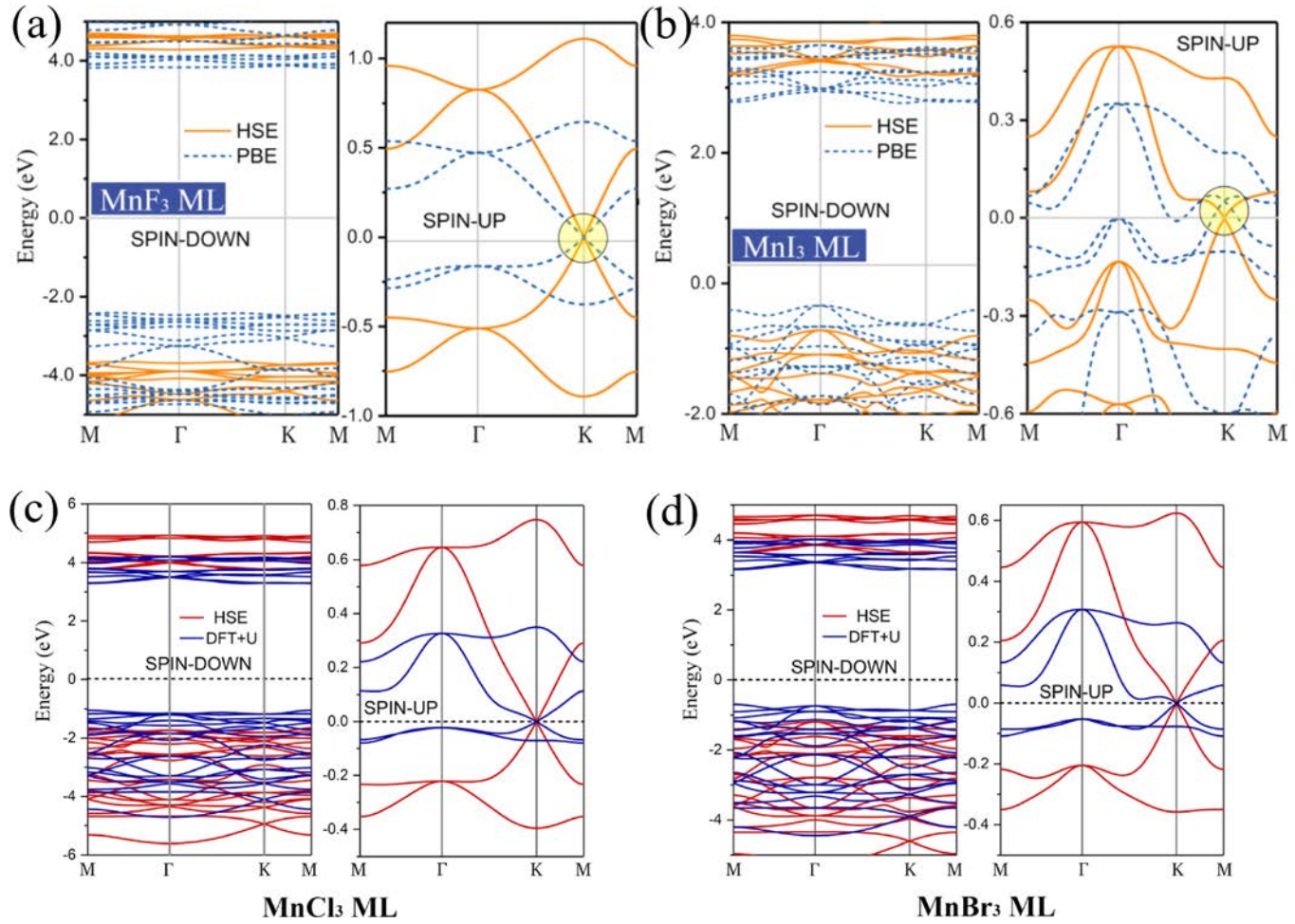

FIG. 17. Spin-resolved band structures of MnX_3 (X = F, Cl, Br, and I) calculated by the HSE06, DFT + U, and PBE methods. Figures are reproduced with permission from Sun *et al.*, Phys. Rev. B **97**(9), 094408 (2018). Copyright 2018 American Physical Society.

g-$C_{14}N_{12}$ and g-$C_{10}N_9$, as shown in Fig. 18. Both frameworks were built as honeycomb lattices using s-triazine and carbon-rich tri-s-tri-azine (C_7N_6) via C-C covalent bonds without sp^2-hybridized nitrogen (or carbon) atoms. Both frameworks have fully spin-polarized ground states. The band structures and DOS spectrum are shown in Fig. 18. In the spin-down channel, g-$C_{14}N_{12}$ can clearly be seen to possess a linear energy dispersion; its Dirac point is truly located at the Fermi level. The band structure in the spin-down channel of g-$C_{10}N_9$ is also displayed, but it possesses a parabolic one. In the spin-up channel, the gaps between the bands are 2.47 and 2.07 eV, respectively. Thus, only g-$C_{14}N_{12}$ can be referred to as a DSGS, g-$C_{10}N_9$ is not. The v_F values of two materials were identical according to calculations, at about 0.82×10^5 m/s. As in the examples discussed in Sec. IV C 4, such a system may have high carrier mobility, indicating its potential for high-efficiency spin transport applications.

The calculated formation energies reveal that both frameworks are energetically stable with respect to g-C_6N_6, which has been synthesized experimentally. Meanwhile, the phonon spectrum analysis confirmed their dynamic stability. Moreover, researchers adopted the supercell to carry out computations. The energy differences between the FM and AFM states of g-$C_{14}N_{12}$ were obtained and showed a robust FM state. Furthermore, using MC simulations combined with heat capacity (C_V) values, a T_C value for g-$C_{14}N_{12}$ of approximately 830 K was obtained. Such a high T_C is enough to prove its thermal stability at room temperature.

When the SOC was taken into account, a small gap appeared between the Dirac cones, potentially enabling this system to achieve the QAH state. Its topological nontriviality was checked by integrating Berry curvature and characterized by *C*. In this case, g-$C_{14}N_{12}$ may be regarded as a Chern insulator. Last but not least, although the SOC gap can be detected at temperatures lower than only 43 K, this temperature is still much higher than required for other materials (30 mK), according to a recent experiment work.[99]

B. YN_2 monolayer

Generally, the DSGSs containing TM elements belong to the *d*-state type, owing to the major contribution to the Dirac states being from the *d*-orbitals of TM atoms, near the Fermi level. Very recently, Liu *et al.*[100] proposed a YN_2 monolayer with octahedral coordination as a *p*-state DSGS using first-principles calculations.

Following the experimental synthesis of MoN_2[101] and the increasing interest in TMN_2 compounds,[102] the intrinsically half-metallic YN_2 has been considered a promising candidate for Dirac materials. Previous studies have shown

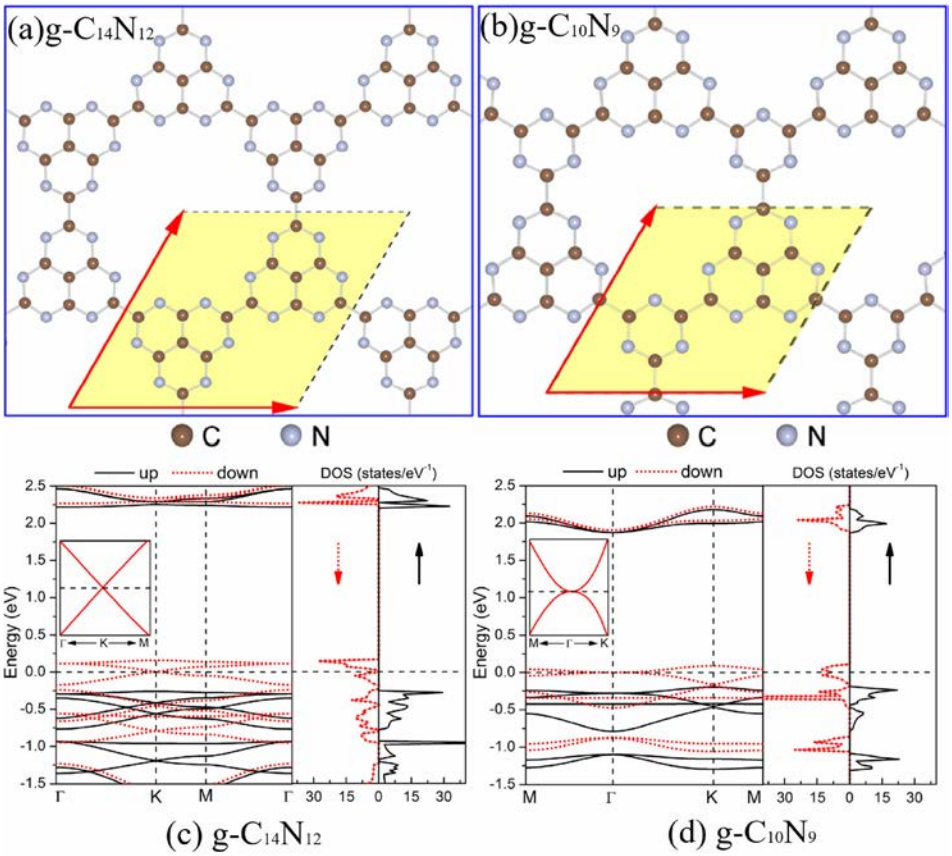

FIG. 18. (a) and (b) Structure diagrams of g-$C_{14}N_{12}$ and g-$C_{10}N_9$, respectively. The unit cells are indicated by the yellow region. (c) and (d) Band structures and total DOS of g-$C_{14}N_{12}$ and g-$C_{10}N_9$, respectively. Figures are reproduced with permission from Zhang *et al.*, Carbon **84**, 1–8 (2015). Copyright 2015 Elsevier Publications.

that its 1 T polymorph was energetically and dynamically stable. Hence, Liu *et al*. adopted such polymorph, which is displayed in Fig. 19(a), for use in their calculations.

The stability of 1T-YN_2 was investigated in detail. The absence of the imaginary frequency indicates the dynamical stability of the 1T-YN_2 monolayer, as shown in Fig. 19(b). Spin-polarized AIMD simulation of a $5 \times 5 \times 1$ supercell with a Nosé-Hoover thermostat at 300 K was carried out. The results confirmed that no structural destruction existed in the monolayer, except for some thermal-induced fluctuations, indicating that 1T-YN_2 is thermally stable at room temperature. To investigate the mechanical stability, as for a 2D material, the effects of lattice distortion on structural stability were assessed. As expected, the 1T-YN_2 sheets had adequate resistance to external strain, and avoided the lattice mismatch caused by substrates.

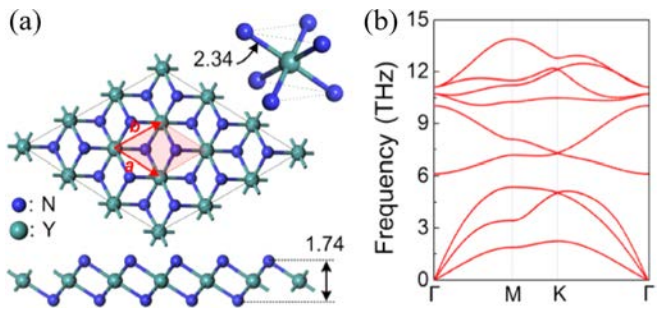

FIG. 19. (a) Structure diagram of the 1T-YN_2 monolayer. The unit cell is indicated by the red region. The octahedral structure unit is displayed in the top inset. (b) The corresponding phonon spectrum shows no imaginary frequency, indicating its synthetic determinacy in the laboratory. Figures are reproduced with permission from Liu *et al.*, Nano Res. **10**(6), 1972–1979 (2017). Copyright 2017 Springer Publications.

The spin-resolved band structures are presented in Fig. 20(a). In the spin-down channel, the band structure can be seen to possess typical gapless features with a linear energy dispersion. In the spin-up channel, the large gap of 4.57 eV is similar to that of a semiconductor. The same DSGS properties were clearly revealed in the band structure illustrations from the three different methods, i.e., PBE, GGA + U, and HSE06. Such canonical features classify the 1T-YN_2 monolayer as a DSGS. Meanwhile, the origins of Dirac states of the monolayer were explored using the PDOS spectra [Fig. 20(b)]. These showed that mainly the N atoms rather than the Y atoms contribute to its Dirac states near the Fermi level, confirming the *p*-state classification of the monolayer. The v_F value, of about 3.70×10^5 m/s, obtained for the 1T-YN_2 monolayer, was considerably higher than those of almost all the Dirac materials [in Fig. 20(d)], and was even comparable to silicene 5.30×10^5 m/s. Thus, the current monolayer could have potential applications in spintronic devices.

Another important parameter that should be considered is T_C, which is used to evaluate the stability of ferromagnetism. Using mean field approximation (MFA), the authors gave a rough estimate of T_C, in the range from 650 K to 1613 K, which was insufficient. They used the empirical relation[103] $T_C/T^{MFA} = 0.51$ to reduce it into the range of 332–823 K, indicating that the FM state was robust enough at room temperature.

For experimental synthesis, the usual method is mechanical exfoliation. Therefore, the cleavage energy of 1T-YN_2

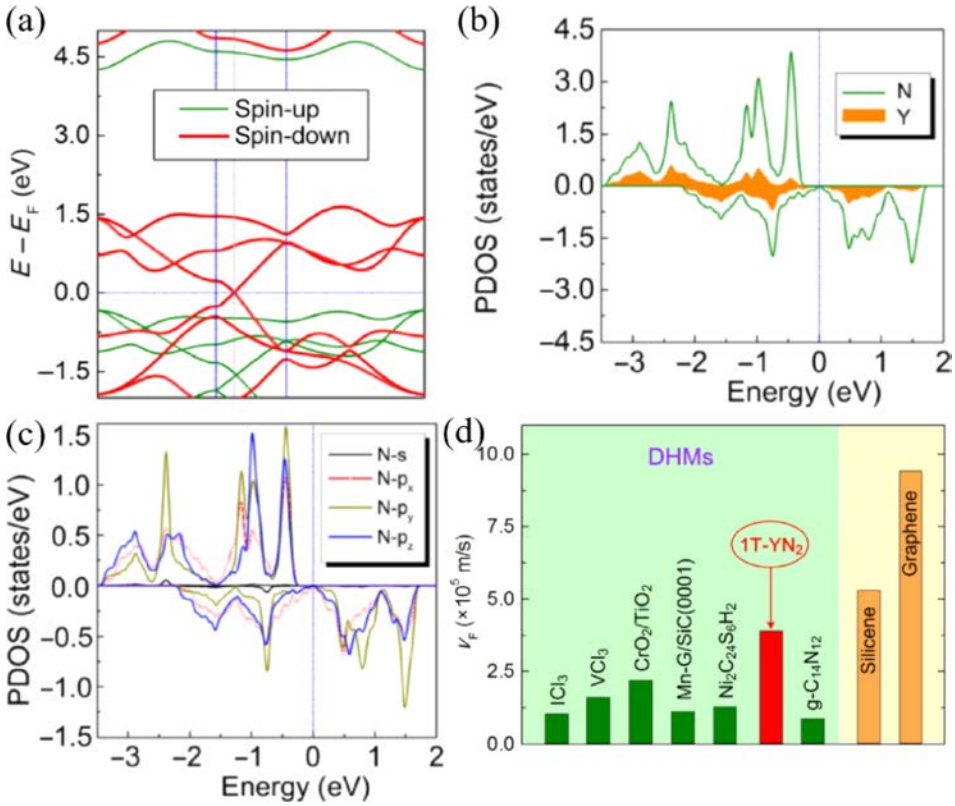

FIG. 20. (a) Band structure of the 1T-YN_2 monolayer. (b) PDOS of the N and Y atoms for the 1T-YN_2 monolayer. (c) PDOS of *s*- and *p*-orbitals of the N atom. (d) Comparison of the values of Fermi velocity (v_F) between previously reported Dirac materials. Specially, the words of DHMs should prefer to be DSGSs. The energies of the Fermi level for the illustrations were set to zero. Figures are reproduced with permission from Liu *et al.*, Nano Res. **10**(6), 1972–1979 (2017). Copyright 2017 Springer Publications.

bulk phase was calculated to be about 0.69 J/m^2, which is smaller than that of 2D sheets Ca_2N (1.09 J/m^2).[104] On the basis of this comparison, it is very likely that the 1T-YN_2 could be exfoliated from bulk phase in experiment. In other respects, Liu *et al*. also found that the ferromagnetism in the 1T-YN_2 monolayer was robust under the doping and external strains. To ensure extensibility when searching DSGSs, the multilayer 1T-YN_2 materials were taken into account. Compared with the interlayer interaction in the MoN_2 bulk solid, that of the layered YN_2 system is weaker. The interlayer binding energy as a function of interlayer distance is shown in Fig. 21(a), illustrating that the layered YN_2 actually possesses weak van der Waals interaction. Meanwhile, as expected, the multilayer 1T-YN_2 systems were confirmed as *p*-state DSGSs (in Fig. 21).

Finally, the experience of designing such *p*-state DSGSs was also described by Liu *et al*.: (i) the Dirac cones originated from the symmetric arrangement of MG atoms instead of TM atoms and (ii) the *s*- or *p*-orbitals, rather than the *d*-orbitals, of open-shell non-metal atoms should be spin-polarized by orbital hybridization. These two principles may provide fundamental guidance for establishing new and meaningful *p*-state DSGSs. The other TM nitrides monolayer, such as scandium dinitrides and lanthanide dinitrides, also deserved to be investigated.

VI. OUTLOOK AND CONCLUSION

In this review article, we first introduced the computational algorithms and presented our own suggestion about clarifying the conceptual distinction between DSGSs and DHMs. Then, we reviewed the recent advances in DSGSs in detail. As promising candidates for future spintronic applications, DSGSs show massless fermions around the Fermi level, ideal dissipation-less properties, and 100% spin-polarization. Moreover, if the rare multiple rings combined by Dirac nodes exist in a DSGS system, it will exhibit more intensive nonlinear electromagnetic responses than a single Dirac cone. It is also important that almost all of the DSGSs possess a high Curie temperature and a robust FM state at room temperature. Meanwhile, owing to topological non-triviality, the QAHE and QSHE will be achieved when considering the SOC, as well as its transition to Chern insulator or Chern half-metal.

Until now, on the basis of past findings, research about DSGS is mainly consisted of theoretical predictions, but these are still very limited. Only a few materials—namely, 2D graphitic nitrides and some TM nitride layered materials—have been demonstrated to be *p*-state DSGSs, while the other materials are *d*-state. The *p*-state DSGSs merit more attention owing to their advantages in high-speed spintronics. To address this issue, Liu *et al*.[100] made two suggestions about designing *p*-state DSGSs for guidelines, which we mentioned in the review about YN_2 monolayer, and may provide new directions in the hunt for potential *p*-state materials. The excellent properties possessed by *d*-state MnF_3 indicate that, in spite of some unique characteristics possessed by *p*-state DSGSs, the *d*-state DSGS are of equal importance and should also be investigated. Furthermore, at present, the search for DSGS appears to be focused on layered materials, on the basis of our review of previous reports. The desirable DSGS states found in the MnF_3 bulk phase should remind researchers that DSGS states can also be found in bulk phase, where they may have even more attractive properties.

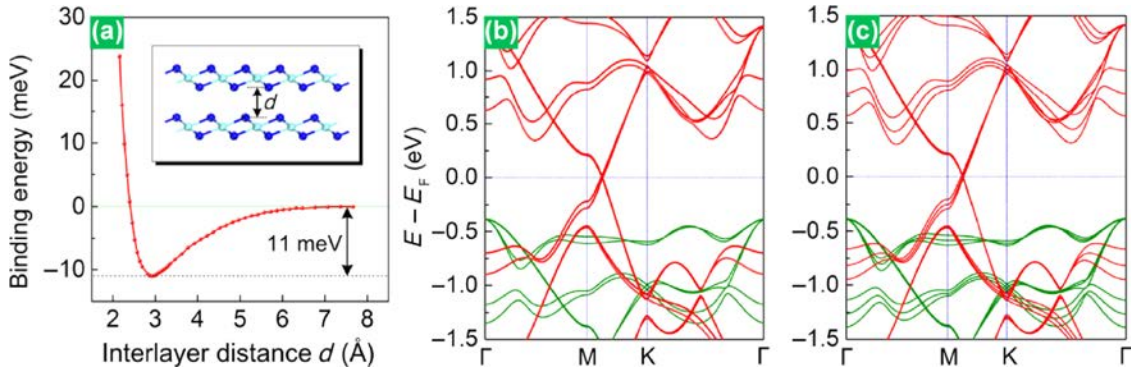

FIG. 21. (a) The binding energy as a function of interlayer distance *d*. (b) and (c) The band structures of bilayer YN_2 and trilayer YN_2, respectively. Figures are reproduced with permission from Liu *et al.*, Nano Res. **10**(6), 1972–1979 (2017). Copyright 2017 Springer Publications.

Theoretical studies, of course, are necessary, but experimental work is more important. Regrettably, only MnF_3 bulk has been synthesized in experiment until now. On the other hand, Gao *et al.*[65] realized Dirac states in Mn-intercalated epitaxial graphene under different coverage of Mn atoms, the Mn-intercalated epitaxial graphene was demonstrated experimentally to be in the DHM state, rather than the truly stable DSGS state. Fortunately, the theoretical work by Li *et al.*[64] in 2015 confirmed that substrate modulation could make its DHM state transform to DSGS state. We think the following experimental work, which is about achieving true DSGS state by coverage modulation in Mn-intercalated epitaxial graphene on SiC (0001), is still meaningful. Additionally, to achieve further advances in the search for DSGSs that can be synthesized experimentally, we suggest that researchers consider the synthetic potential of compounds such as the 2D graphitic carbon nitrides,[98] TM halides,[80,81,87,90] and simple oxide heterostructures,[69] which are usually built into either honeycomb lattices or cubic types according to computations. The structural designs of these materials are all based on further explorations in well-known traditional compounds (such as tri-s-tri-azine, TMF_3, and the CrO_2/TiO_2 heterostructures), which have been widely synthesized and used by chemists for a long time. Besides, some reports[75,80,90,100] suggest that mechanical exfoliation may play an significant part in practical synthesis, especially its successful application for graphene. In short, to demonstrate the feasibility of these theoretical results, it is desirable for researchers to follow such reports[75,80,90,100] with experiments.

Despite being important members of the SGS family, Heusler compounds have been absent from the DSGS family. There have been no reports of studies focusing on Heusler compounds in the search for new DSGS. We have made some efforts in this direction in our recent work, where we found that quasi-linear SGS behavior can be found in 3D Heusler compounds. The band structures and the phonon spectrum of a half-Heusler-type KCrTe compound are given in Fig. 22, illustrating its quasi-linear SGS properties and structural stability. Similar to the first synthesized PSGS Mn_2CoAl,[20] we hope new DSGSs can be found among Heusler compounds and their DSGS properties can be confirmed in the near future.

DSGSs are likely to be a focus of future research, both as a promising platform for spintronics, and owing to their other properties such as spin transport and thermal spin transport, which will be of interest to researchers.

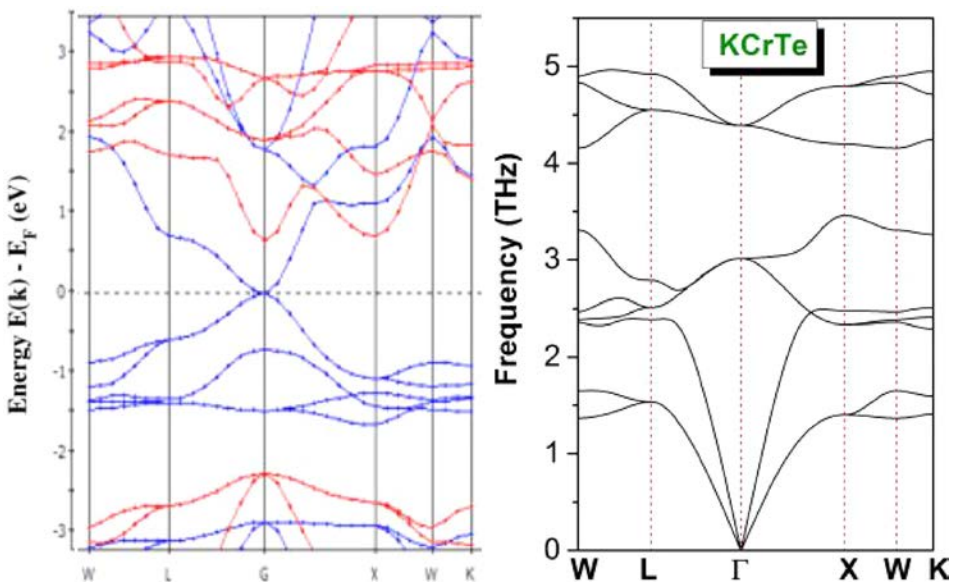

FIG. 22. Band structure of KCrTe and its corresponding phonon spectrum. The quasi-linear energy dispersion can be clearly seen near the Fermi level. There is no imaginary frequency in the phonon spectrum, indicating its dynamical stability and the plausibility of its synthesis.

ACKNOWLEDGMENTS

Professor Zhengxiang Cheng thanks the Australian Research Council for the support. Dr. Xiaotian Wang thanks the Program for Basic Research and Frontier Exploration of Chongqing City (No. cstc2018jcyjA0765), National Natural Science Foundation of China (No. 51801163), and Doctoral Fund Project of Southwest University (No. 117041) for the support. Tingzhou Li and Dr. Xiaotian Wang thank Dr. Liying Wang (Tianjin University), Professor Rabah Khenata (Mascara University) for the useful discussions and Professor A. Bouhemadou (University Ferhat Abbas Setif 1) for calculating the phonon dispersion curves for KCrTe in Fig. 22. The authors declare no conflict of interest.

[1]X. Li and J. Yang, "First-principles design of spintronics materials," Natl. Sci. Rev. **3**(3), 365–381 (2016).
[2]D. D. Awschalom and M. E. Flatté, "Challenges for semiconductor spintronics," Nat. Phys. **3**(3), 153 (2007).
[3]C. Felser, G. H. Fecher, and B. Balke, "Spintronics: A challenge for materials science and solid-state chemistry," Angew. Chem. Int. Ed. **46**(5), 668–699 (2007).
[4]R. A. De Groot, F. M. Mueller, P. G. Van Engen *et al.*, "New class of materials: Half-metallic ferromagnets," Phys. Rev. Lett. **50**(25), 2024 (1983).
[5]P. Dowben, "Half metallic ferromagnets," J. Phys.: Condens. Matter **19**(31), 310301 (2007).
[6]H. Van Leuken and R. A. De Groot, "Half-metallic antiferromagnets," Phys. Rev. Lett. **74**(7), 1171 (1995).
[7]K. W. Lee and C. E. Lee, "Half-metallic carbon nanotubes," Adv. Mater. **24**(15), 2019–2023 (2012).
[8]I. Galanakis and E. Şaşıoğlu, "High T_C half-metallic fully-compensated ferrimagnetic Heusler compounds," Appl. Phys. Lett. **99**(5), 052509 (2011).
[9]D. Hsieh, D. Qian, L. Wray *et al.*, "A topological Dirac insulator in a quantum spin Hall phase," Nature **452**(7190), 970 (2008).
[10]J. Moore, "Topological insulators: The next generation," Nat. Phys. **5**(6), 378 (2009).
[11]Y. Xia, D. Qian, D. Hsieh *et al.*, "Observation of a large-gap topological-insulator class with a single Dirac cone on the surface," Nat. Phys. **5**(6), 398 (2009).
[12]Y. S. Hor, A. Richardella, P. Roushan *et al.*, "p-type Bi_2Se_3 for topological insulator and low-temperature thermoelectric applications," Phys. Rev. B **79**(19), 195208 (2009).
[13]Y. L. Chen, J. G. Analytis, J. H. Chu *et al.*, "Experimental realization of a three-dimensional topological insulator, Bi_2Te_3," Science **325**(5937), 178–181 (2009).
[14]D. Hsieh, Y. Xia, D. Qian *et al.*, "Observation of time-reversal-protected single-Dirac-cone topological-insulator states in Bi_2Te_3 and Sb_2Te_3," Phys. Rev. Lett. **103**(14), 146401 (2009).
[15]H. Ohno, A. Shen, F. Matsukura *et al.*, "Ga, Mn)As: A new diluted magnetic semiconductor based on GaAs," Appl. Phys. Lett. **69**(3), 363–365 (1996).(
[16]H. Kimura, T. Fukumura, M. Kawasaki *et al.*, "Rutile-type oxide-diluted magnetic semiconductor: Mn-doped SnO_2," Appl. Phys. Lett. **80**(1), 94–96 (2002).
[17]A. Ramasubramaniam and D. Naveh, "Mn-doped monolayer MoS_2: An atomically thin dilute magnetic semiconductor," Phys. Rev. B **87**(19), 195201 (2013).
[18]R. Q. Wu, G. W. Peng, L. Liu *et al.*, "Cu-doped GaN: A dilute magnetic semiconductor from first-principles study," Appl. Phys. Lett. **89**(6), 062505 (2006).
[19]X. L. Wang, "Proposal for a new class of materials: Spin gapless semiconductors," Phys. Rev. Lett. **100**(15), 156404 (2008).
[20]G. D. Liu, X. F. Dai, H. Y. Liu *et al.*, "Mn_2CoZ (Z = Al, Ga, In, Si, Ge, Sn, Sb) compounds: Structural, electronic, and magnetic properties," Phys. Rev. B **77**(1), 014424 (2008).
[21]S. Skaftouros, K. Özdoğan, E. Şaşıoğlu *et al.*, "Search for spin gapless semiconductors: The case of inverse Heusler compounds," Appl. Phys. Lett. **102**(2), 022402 (2013).
[22]L. Wang and Y. J. Jin, "A spin-gapless semiconductor of inverse Heusler Ti_2CrSi alloy: First-principles prediction," J. Magn. Magn. Mater. **385**(1), 55–59 (2015).
[23]H. Y. Jia, X. F. Dai, L. Y. Wang, R. Liu, X. T. Wang, P. P. Li, Y. T. Cui, and G. D. Liu, "Doping effect on electronic structures and bandgap of inverse Heusler compound: Ti_2CrSn," J. Magn. Magn. Mater. **367**, 33–39 (2014).
[24]G. Y. Gao and K. L. Yao, "Antiferromagnetic half-metals, gapless half-metals, and spin gapless semiconductors: The $D0_3$-type Heusler alloys," Appl. Phys. Lett. **103**(23), 232409 (2013).
[25]Y. Pan and Z. Yang, "Exploration of magnetism in armchair graphene nanoribbons with radical groups," Chem. Phys. Lett. **518**, 104–108 (2011).
[26]Y. Li, Z. Zhou, P. Shen *et al.*, "Spin gapless semiconductor-metal-half-metal properties in nitrogen-doped zigzag graphene nanoribbons," ACS Nano **3**(7), 1952–1958 (2009).
[27]Z. F. Wang, S. Jin, and F. Liu, "Spatially separated spin carriers in spin-semiconducting graphene nanoribbons," Phys. Rev. Lett. **111**(9), 096803 (2013).
[28]J. He, P. Zhou, N. Jiao *et al.*, "Half-Semiconductor antiferromagnets and spin-gapless-semiconductor antiferromagnets," pre-print arXiv:1308.0253 (2013).
[29]S. D. Guo and B. G. Liu, "Density-functional-theory investigation of pressure induced semiconductor-metal transitions in the ferromagnetic semiconductor $HgCr_2Se_4$," J. Phys.: Condens. Matter **24**(4), 045502 (2012).
[30]Y. Pan and Z. Yang, "Electronic structures and spin gapless semiconductors in BN nanoribbons with vacancies," Phys. Rev. B **82**(19), 195308 (2010).
[31]L. Y. Wang, X. F. Dai, X. T. Wang *et al.*, "Single spin channels in Fe-doped CoTiSb semiconductor," Superlattices Microstruct. **83**, 261–270 (2015).
[32]L. Bainsla, A. I. Mallick, M. M. Raja *et al.*, "Origin of spin gapless semiconductor behavior in CoFeCrGa: Theory and experiment," Phys. Rev. B **92**(4), 045201 (2015).
[33]G. Z. Xu, E. K. Liu, Y. Du *et al.*, "A new spin gapless semiconductors family: Quaternary Heusler compounds," EPL (Europhys. Lett.) **102**(1), 17007 (2013).
[34]Q. Gao, H. H. Xie, L. Li *et al.*, "First-principle study on some new spin-gapless semiconductors: The Zr-based quaternary Heusler alloys," Superlattices Microstruct. **85**, 536–542 (2015).
[35]X. Wang, Z. Cheng, G. Liu *et al.*, "Rare earth-based quaternary Heusler compounds MCoVZ (M = Lu, Y; Z= Si, Ge) with tunable band characteristics for potential spintronic applications," IUCrJ **4**(6), 758–768 (2017).
[36]H. M. Huang, Z. Y. Jiang, Y. M. Lin *et al.*, "Design of half-metal and spin gapless semiconductor for spintronics application via cation substitution in methylammonium lead iodide," Appl. Phys. Express **10**(12), 123002 (2017).
[37]Y. Li, Y. Ma, M. Zhao *et al.*, "The magnetism of intrinsic structural defects in monolayer $MoTe_2$," J. Alloys Compd. **735**, 2363–2372 (2018).
[38]S. Ouardi, G. H. Fecher, C. Felser *et al.*, "Realization of spin gapless semiconductors: The Heusler compound Mn_2CoAl," Phys. Rev. Lett. **110**(10), 100401 (2013).
[39]F. Zheng, C. Zhang, P. Wang *et al.*, "Novel half-metal and spin gapless semiconductor properties in N-doped silicene nanoribbons," J. Appl. Phys. **113**(15), 154302 (2013).
[40]G. Gao, G. Ding, J. Li *et al.*, "Monolayer MXenes: Promising half-metals and spin gapless semiconductors," Nanoscale **8**(16), 8986–8994 (2016).
[41]W. Feng, X. Fu, C. Wan *et al.*, "Spin gapless semiconductor like Ti_2MnAl film as a new candidate for spintronics application," Phys. Status Solidi (RRL) **9**(11), 641–645 (2015).
[42]P. Lukashev, P. Kharel, S. Gilbert *et al.*, "Investigation of spin-gapless semiconductivity and half-metallicity in Ti_2MnAl-based compounds," Appl. Phys. Lett. **108**(14), 141901 (2016).
[43]X. Yang, X. Wu, B. Wu *et al.*, "First-principles calculated spin-gapless semiconducting behavior in quaternary VCoHfGa and CrFeHfGa Heusler compounds," Mater. Sci. Eng. B **209**, 45–50 (2016).
[44]J. Zhao, H. Liu, Z. Yu *et al.*, "Rise of silicene: A competitive 2D material," Prog. Mater. Sci. **83**, 24–151 (2016).
[45]J. Kim, S. S. Baik, S. H. Ryu *et al.*, "Observation of tunable bandgap and anisotropic Dirac semimetal state in black phosphorus," Science **349**(6249), 723–726 (2015).

[46]L. Z. Zhang, Z. F. Wang, S. X. Du *et al.*, "Prediction of a Dirac state in monolayer TiB_2," Phys. Rev. B **90**(16), 161402 (2014).
[47]M. E. Dávila and G. Le Lay, "Few layer epitaxial germanene: A novel two-dimensional Dirac material," Sci. Rep. **6**, 20714 (2016).
[48]W. Yang and P. W. Ayers, *Density-Functional Theory: Computational Medicinal Chemistry for Drug Discovery* (CRC Press, 2003), pp. 103-132.
[49]B. Delley, "DMol^3 DFT studies: From molecules and molecular environments to surfaces and solids," Comput. Mater. Sci. **17**(2-4), 122–126 (2000).
[50]Ordejón P, Sánchez-Portal D, Artacho E, *et al.* SIESTA: Spanish Initiative for Electronic Simulations with Thousands of Atoms. http://www.uam.es/siesta (2001).
[51]J. Hafner, "Ab-initio simulations of materials using VASP: Density-functional theory and beyond," J. Comput. Chem. **29**(13), 2044–2078 (2008).
[52]M. D. Segall, P. J. D. Lindan, M. J. Probert *et al.*, "First-principles simulation: Ideas, illustrations and the CASTEP code," J. Phys.: Condens. Matter **14**(11), 2717 (2002).
[53]X. Gonze, J. M. Beuken, R. Caracas *et al.*, "First-principles computation of material properties: The ABINIT software project," Comput. Mater. Sci. **25**(3), 478–492 (2002).
[54]P. Giannozzi, S. Baroni, N. Bonini *et al.*, "QUANTUM ESPRESSO: A modular and open-source software project for quantum simulations of materials," J. Phys.: Condens. Matter **21**(39), 395502 (2009).
[55]D. C. Langreth and M. J. Mehl, "Beyond the local-density approximation in calculations of ground-state electronic properties," Phys. Rev. B **28**(4), 1809 (1983).
[56]J. P. Perdew, K. Burke, and M. Ernzerhof, "Generalized gradient approximation made simple," Phys. Rev. Lett. **77**(18), 3865 (1996).
[57]K. Burke, J. P. Perdew, and Y. Wang, *Derivation of a Generalized Gradient Approximation: The PW91 Density Functional: Electronic Density Functional Theory* (Springer, Boston, MA, 1998), pp. 81-111.
[58]M. Ernzerhof and G. E. Scuseria, "Assessment of the Perdew-Burke-Ernzerhof exchange-correlation functional," J. Chem. Phys. **110**(11), 5029–5036 (1999).
[59]M. Tas, E. Şaşıoğlu, C. Friedrich *et al.*, "A first-principles DFT+ GW study of spin-filter and spin-gapless semiconducting Heusler compounds," J. Magn. Magn. Mater. **441**, 333–338 (2017).
[60]J. Heyd and G. E. Scuseria, "Efficient hybrid density functional calculations in solids: Assessment of the Heyd-Scuseria-Ernzerhof screened Coulomb hybrid functional," J. Chem. Phys. **121**(3), 1187–1192 (2004).
[61]G. Dresselhaus, "Spin-orbit coupling effects in zinc blende structures," Phys. Rev. **100**(2), 580 (1955).
[62]M. Galvan, A. Vela, and J. L. Gazquez, "Chemical reactivity in spin-polarized density functional theory," J. Phys. Chem. **92**(22), 6470–6474 (1988).
[63]X. Wang, Z. Cheng, J. Wang *et al.*, "Recent advances in the Heusler based spin-gapless semiconductors," J. Mater. Chem. C **4**(30), 7176–7192 (2016).
[64]Y. Li, D. West, H. Huang *et al.*, "Theory of the Dirac half metal and quantum anomalous Hall effect in Mn-intercalated epitaxial graphene," Phys. Rev. B **92**(20), 201403 (2015).
[65]T. Gao, Y. Gao, C. Chang *et al.*, "Atomic-scale morphology and electronic structure of manganese atomic layers underneath epitaxial graphene on SiC (0001)," ACS Nano **6**(8), 6562–6568 (2012).
[66]K. Schwarz, "CrO_2 predicted as a half-metallic ferromagnet," J. Phys. F: Met. Phys. **16**(9), L211 (1986).
[67]G. Y. Gao, K. L. Yao, Z. L. Liu *et al.*, "Half-metallic ferromagnetism of Cr-doped rutile TiO_2: A first-principles pseudopotential study," Phys. B: Condens. Matter **382**(1-2), 14–16 (2006).
[68]J. M. D. Coey and M. Venkatesan, "Half-metallic ferromagnetism: Example of CrO_2," J. Appl. Phys. **91**(10), 8345–8350 (2002).
[69]T. Cai, X. Li, F. Wang *et al.*, "Single-spin Dirac fermion and Chern insulator based on simple oxides," Nano Lett. **15**(10), 6434–6439 (2015).
[70]H. M. Huang, Z. W. Zhu, C. K. Zhang *et al.*, "First principles investigation of half-metallicity and spin gapless semiconductor in $CH_3NH_3Cr_xPb_{1-x}I_3$ mixed perovskites," Appl. Phys. A **124**(4), 284 (2018).
[71]K. Sumida, D. L. Rogow, J. A. Mason *et al.*, "Carbon dioxide capture in metal-organic frameworks," Chem. Rev. **112**(2), 724–781 (2012).
[72]J. R. Li, J. Yu, W. Lu *et al.*, "Porous materials with pre-designed single-molecule traps for CO_2 selective adsorption," Nat. Commun. **4**, 1538 (2013).
[73]Y. Ma, Y. Dai, W. Wei *et al.*, "Novel two-dimensional tetragonal monolayer: metal-TCNQ networks," J. Phys. Chem. A **117**(24), 5171–5177 (2013).
[74]Z. F. Wang, Z. Liu, and F. Liu, "Quantum anomalous Hall effect in 2D organic topological insulators," Phys. Rev. Lett. **110**(19), 196801 (2013).
[75]Y. Ma, Y. Dai, X. Li *et al.*, "Prediction of two-dimensional materials with half-metallic Dirac cones: $Ni_2C_{18}H_{12}$ and $Co_2C_{18}H_{12}$," Carbon **73**, 382–388 (2014).
[76]K. Lee and G. A. Sotzing, "Poly (thieno, [3,4-b] thiophene): A new stable low bandgap conducting polymer," Macromolecules **34**(17), 5746–5747 (2001).
[77]L. Wei, X. Zhang, and M. Zhao, "Spin-polarized Dirac cones and topological nontriviality in a metal-organic framework $Ni_2C_{24}S_6H_{12}$," Phys. Chem. Chem. Phys. **18**(11), 8059–8064 (2016).
[78]X. Hu, M. Kargarian, and G. A. Fiete, "Topological insulators and fractional quantum Hall effect on the ruby lattice," Phys. Rev. B **84**(15), 155116 (2011).
[79]A. Wang, X. Zhang, Y. Feng *et al.*, "Chern insulator and Chern half-metal states in the two-dimensional spin-gapless semiconductor $Mn_2C_6S_{12}$," J. Phys. Chem. Lett. **8**(16), 3770–3775 (2017).
[80]J. He, S. Ma, P. Lyu *et al.*, "Unusual Dirac half-metallicity with intrinsic ferromagnetism in vanadium trihalide monolayers," J. Mater. Chem. C **4**(13), 2518–2526 (2016).
[81]J. He, X. Li, P. Lyu *et al.*, "Near-room-temperature Chern insulator and Dirac spin-gapless semiconductor: Nickel chloride monolayer," Nanoscale **9**(6), 2246–2252 (2017).
[82]C. Hwang, D. A. Siegel, S. K. Mo *et al.*, "Fermi velocity engineering in graphene by substrate modification," Sci. Rep. **2**, 590 (2012).
[83]M. A. Hepworth and K. H. Jack, "The crystal structure of manganese trifluoride, MnF_3," Acta Crystallogr. **10**(5), 345–351 (1957).
[84]Z. Mazej, "Room temperature syntheses of MnF_3, MnF_4 and hexafluoromanganete (IV) salts of alkali cations," J. Fluorine Chem. **114**(1), 75–80 (2002).
[85]J. Yuan, X. Yan, C. Dai *et al.*, "Electronic and magnetic properties of monolayer WS_2 doped with MnX_m (m = 0, 3, 6; X = N, O, F)," Surf. Rev. Lett. **22**(06), 1550071 (2015).
[86]X. Zhang, D. Li, J. Meng *et al.*, "Electronic and magnetic properties of $MnF_{3(4)}$ superhalogen cluster-sandwiched bilayer graphene: First-principles calculations," Comput. Mater. Sci. **124**, 316–322 (2016).
[87]Y. Jiao, F. Ma, C. Zhang *et al.*, "First-principles prediction of spin-polarized multiple Dirac rings in manganese fluoride," Phys. Rev. Lett. **119**(1), 016403 (2017).
[88]F. Ma, Y. Jiao, G. Gao *et al.*, "Graphene-like two-dimensional ionic boron with double Dirac cones at ambient condition," Nano Lett. **16**(5), 3022–3028 (2016).
[89]Y. Jiao, F. Ma, J. Bell *et al.*, "Two-dimensional boron hydride sheets: High stability, massless Dirac fermions, and excellent mechanical properties," Angew. Chem. **128**(35), 10448–10451 (2016).
[90]Q. Sun and N. Kioussis, "Prediction of manganese trihalides as two-dimensional Dirac half-metals," Phys. Rev. B **97**(9), 094408 (2018).
[91]W. Wei and T. Jacob, "Strong excitonic effects in the optical properties of graphitic carbon nitride g-C_3N_4 from first principles," Phys. Rev. B **87**(8), 085202 (2013).
[92]A. B. Jorge, D. J. Martin, M. T. S. Dhanoa *et al.*, "H_2 and O_2 evolution from water half-splitting reactions by graphitic carbon nitride materials," J. Phys. Chem. C **117**(14), 7178–7185 (2013).
[93]X. Wang, K. Maeda, A. Thomas *et al.*, "A metal-free polymeric photocatalyst for hydrogen production from water under visible light," Nat. Mater. **8**(1), 76 (2009).
[94]X. Wang, S. Blechert, and M. Antonietti, "Polymeric graphitic carbon nitride for heterogeneous photocatalysis," ACS Catal. **2**(8), 1596–1606 (2012).
[95]Y. Wang, X. Wang, and M. Antonietti, "Polymeric graphitic carbon nitride as a heterogeneous organocatalyst: From photochemistry to multipurpose catalysis to sustainable chemistry," Angew. Chem. Int. Ed. **51**(1), 68–89 (2012).
[96]M. Groenewolt and M. Antonietti, "Synthesis of g-C_3N_4 nanoparticles in mesoporous silica host matrices," Adv. Mater. **17**(14), 1789–1792 (2005).

[97]J. S. Lee, X. Wang, H. Luo *et al*., "Fluidic carbon precursors for formation of functional carbon under ambient pressure based on ionic liquids," Adv. Mater. **22**(9), 1004–1007 (2010).
[98]X. Zhang, A. Wang, and M. Zhao, "Spin-gapless semiconducting graphitic carbon nitrides: A theoretical design from first principles," Carbon **84**, 1–8 (2015).
[99]C. Z. Chang, J. Zhang, X. Feng *et al*., "Experimental observation of the quantum anomalous Hall effect in a magnetic topological insulator," Science **340**, 167–170 (2013).
[100]Z. Liu, J. Liu, and J. Zhao, "YN_2 monolayer: Novel p-state Dirac half metal for high-speed spintronics," Nano Res. **10**(6), 1972–1979 (2017).
[101]S. Wang, H. Ge, S. Sun *et al*., "A new molybdenum nitride catalyst with rhombohedral MoS_2 structure for hydrogenation applications," J. Am. Chem. Soc. **137**(14), 4815–4822 (2015).
[102]F. Wu, C. Huang, H. Wu *et al*., "Atomically thin transition-metal dinitrides: High-temperature ferromagnetism and half-metallicity," Nano Lett. **15**(12), 8277–8281 (2015).
[103]N. W. Ascroft and D. Mermin, *Solid State Physics* (Holt, Rinehart and Winston, New York, 1976).
[104]S. Zhao, Z. Li, and J. Yang, "Obtaining two-dimensional electron gas in free space without resorting to electron doping: An electride based design," J. Am. Chem. Soc. **136**(38), 13313-1331 (2014).